RESEARCH ARTICLE

CXCR4^{high} megakaryocytes regulate host-defense immunity against bacterial pathogens

Jin Wang[1†], Jiayi Xie[2,3†], Daosong Wang[3†], Xue Han[2,3†], Minqi Chen[3], Guojun Shi[1*], Linjia Jiang[2*], Meng Zhao[2,3*]

[1]Department of Endocrinology & Metabolism, The Third Affiliated Hospital, Sun Yat-sen University, Guangzhou, China; [2]RNA Biomedical Institute, Sun Yat-sen Memorial Hospital, Sun Yat-sen University, Guangzhou, China; [3]Key Laboratory of Stem Cells and Tissue Engineering, Zhongshan School of Medicine, Sun Yat-sen University, Ministry of Education, Guangzhou, China

Abstract Megakaryocytes (MKs) continuously produce platelets to support hemostasis and form a niche for hematopoietic stem cell maintenance in the bone marrow. MKs are also involved in inflammatory responses; however, the mechanism remains poorly understood. Using single-cell sequencing, we identified a CXCR4 highly expressed MK subpopulation, which exhibited both MK-specific and immune characteristics. CXCR4^{high} MKs interacted with myeloid cells to promote their migration and stimulate the bacterial phagocytosis of macrophages and neutrophils by producing TNFα and IL-6. CXCR4^{high} MKs were also capable of phagocytosis, processing, and presenting antigens to activate T cells. Furthermore, CXCR4^{high} MKs also egressed circulation and infiltrated into the spleen, liver, and lung upon bacterial infection. Ablation of MKs suppressed the innate immune response and T cell activation to impair the anti-bacterial effects in mice under the *Listeria monocytogenes* challenge. Using hematopoietic stem/progenitor cell lineage-tracing mouse lines, we show that CXCR4^{high} MKs were generated from infection-induced emergency megakaryopoiesis in response to bacterial infection. Overall, we identify the CXCR4^{high} MKs, which regulate host-defense immune response against bacterial infection.

***For correspondence:** shigj6@mail.sysu.edu.cn (GS); jianglj7@mail.sysu.edu.cn (LJ); zhaom38@mail.sysu.edu.cn (MZ)

†These authors contributed equally to this work

Competing interest: The authors declare that no competing interests exist.

Funding: See page 21

Preprinted: 10 June 2021
Received: 15 March 2022
Accepted: 28 July 2022
Published: 29 July 2022

Reviewing Editor: Jalees Rehman, University of Illinois at Chicago, United States

Editor's evaluation

The manuscript by Wang and colleagues studies the heterogeneity of megakaryocytes using single-cell RNA-seq and identifies a subpopulation of CXCR4-high megakaryocytes with immune modulatory roles. Functional studies in this paper show that this subpopulation of megakaryocytes promotes bacterial phagocytosis by macrophages and neutrophils. The compelling evidence for these findings in the manuscript and the fundamental significance of identifying mechanisms by which megakaryocyte subpopulations can impact host defense make this work of interest to researchers in the fields of immunology, hematopoiesis and megakaryocyte biology.

Introduction

Megakaryocytes (MKs) are large and rare hematopoietic cells in the bone marrow, which continually produce platelets to support hemostasis and thrombosis (***Deutsch and Tomer, 2006***). MK progenitors undergo multiple rounds of endomitosis during maturation to achieve polyploidy (***Chang et al., 2007***; ***Deutsch and Tomer, 2013***; ***Machlus and Italiano, 2013***; ***Nagata et al., 1997***; ***Patel et al., 2005***). MKs and their progenitors migrate between distinct microenvironments and organs for their proliferation,

maturation, and biological functions (**Avecilla et al., 2004**; **Fuentes et al., 2010**; **Lefrançais et al., 2017**; **Pal et al., 2020**; **Tamura et al., 2016**; **Wang et al., 1998**). Although platelet generation is the prominent role of MKs, emerging evidence suggests that MKs have other biological functions. Mature MKs interact with HSCs and constitute a unique niche to preserve HSC quiescence in the bone marrow (**Bruns et al., 2014**; **Zhao et al., 2014**). MKs also interact with other niche cells, such as osteoblasts (**Dominici et al., 2009**; **Olson et al., 2013**), non-myelinating Schwann cells (**Jiang et al., 2018**; **Yamazaki et al., 2011**), and blood vessels (**Avecilla et al., 2004**; **Saçma et al., 2019**) to further influence the attraction and retention of hematopoietic stem and progenitor cells during homeostasis and stress.

MK-biased hematopoietic stem cells (HSCs) induce emergency megakaryopoiesis to actively generate MKs upon acute inflammation, which can efficiently replenish the platelet loss during inflammatory insult (**Haas et al., 2015**). Studies suggested that MKs might participate in immune responses independent of their platelet generation role (**Cunin and Nigrovic, 2019**). MKs express multiple immune receptors, such as IgG Fc receptors and toll-like receptors (TLRs), enabling them to sense inflammation directly (**Cunin and Nigrovic, 2019**). Mature MKs also express major histocompatibility complex (MHC) to activate antigen-specific $CD8^+$ T cells and enhance $CD4^+$ T cells and Th17 cell responses through stimulating antigen processing (**Finkielsztein et al., 2015**; **Pariser et al., 2021**; **Zufferey et al., 2017**). Furthermore, MKs release multiple cytokines and chemokines to influence immune cells. For example, MKs produce IL-1α and IL-1β to promote arthritis susceptibility in mice resistant to arthritis (**Cunin et al., 2017**) and produce CXCL1 and CXCL2 to promote neutrophil efflux from the bone marrow (**Köhler et al., 2011**). Lung MKs contribute to thrombosis (**Lefrançais et al., 2017**) and, more interestingly, participate in immune responses (**Pariser et al., 2021**), although the relationship between lung MKs and bone marrow circulating MKs (**Nishimura et al., 2015**) remains unexplored. Furthermore, the recent single-cell atlas shows that MKs are heterogeneous and contain subpopulations that express multiple immune genes and are involved in inflammation response (**Liu et al., 2021**; **Pariser et al., 2021**; **Sun et al., 2021**; **Yeung et al., 2020**). Here, by combining scRNA-seq with functional assays, we identified a $CXCR4^{high}$ MK population, which was generated by infection-induced emergency megakaryopoiesis, and stimulated innate immunity against bacterial infection.

Results

Single-cell atlas identifies an immune-modulatory subpopulation of MKs

We applied droplet-based scRNA-seq with $CD41^+$ forward scatter $(FSC)^{high}$ bone marrow MKs to explore the MK heterogeneity (**Figure 1A**; **Figure 1—figure supplement 1A,B**). To enrich accurate MKs, we further performed transcriptomic profile analysis in the phenotypically enriched MKs (**Yeung et al., 2020**). Our scRNA-seq successfully detected 5368 high-quality cells (**Figure 1—figure supplement 1B,C**), in which one MK cluster (1712 cells) and six immune cell clusters (3656 cells) were annotated according to their gene profile (**Figure 1—figure supplement 1D-G**) and the alignment with published scRNA-seq data (**Almanzar et al., 2020**; **Hamey et al., 2021**; **Pariser et al., 2021**; **Xie et al., 2020**; **Yeung et al., 2020**). Our annotated MKs were similar to MKs but distinct to immune cells, including myeloid progenitors, basophils, neutrophils, monocytes, dendritic cells, macrophages, B cells, and T cells, in an integrated scRNA-seq analysis platform (**Figure 1—figure supplement 2**). Therefore, we re-clustered the transcriptionally enriched 1712 MKs into five subpopulations, termed MK1 to MK5 (**Figure 1B**; **Figure 1—figure supplement 3A,B**), which were further confirmed by the integrated scRNA-seq analysis platform to rule out the potential immune cell contamination (**Pariser et al., 2021**; **Xie et al., 2020**; **Yeung et al., 2020**; **Figure 1—figure supplement 3C,D**). We noticed that mature MKs with huge sizes were captured at a relatively low rate, potentially due to the limitation in current techniques in cell purification and single-cell preparation (**Liu et al., 2021**; **Sun et al., 2021**).

Enriched signature genes by Gene Ontology exhibited that MK1 and MK2 highly expressed nuclear division, DNA replication and repair genes for endomitosis (**Figure 1C,D**). MK3 enriched blood coagulation and thrombosis genes for platelet generation (**Figure 1C,D**). No signature pathways were enriched in MK4. MK5 enriched cell migration and immune response genes (**Figure 1C,D**; **Figure 1—figure supplement 4A-E**), cytokine, chemokine (**Figure 1E,F**; **Figure 1—figure supplement 4F**), and genes involved in immune cell interaction (**Figure 1G**, **Figure 1—figure supplement 5A**). MK5 also

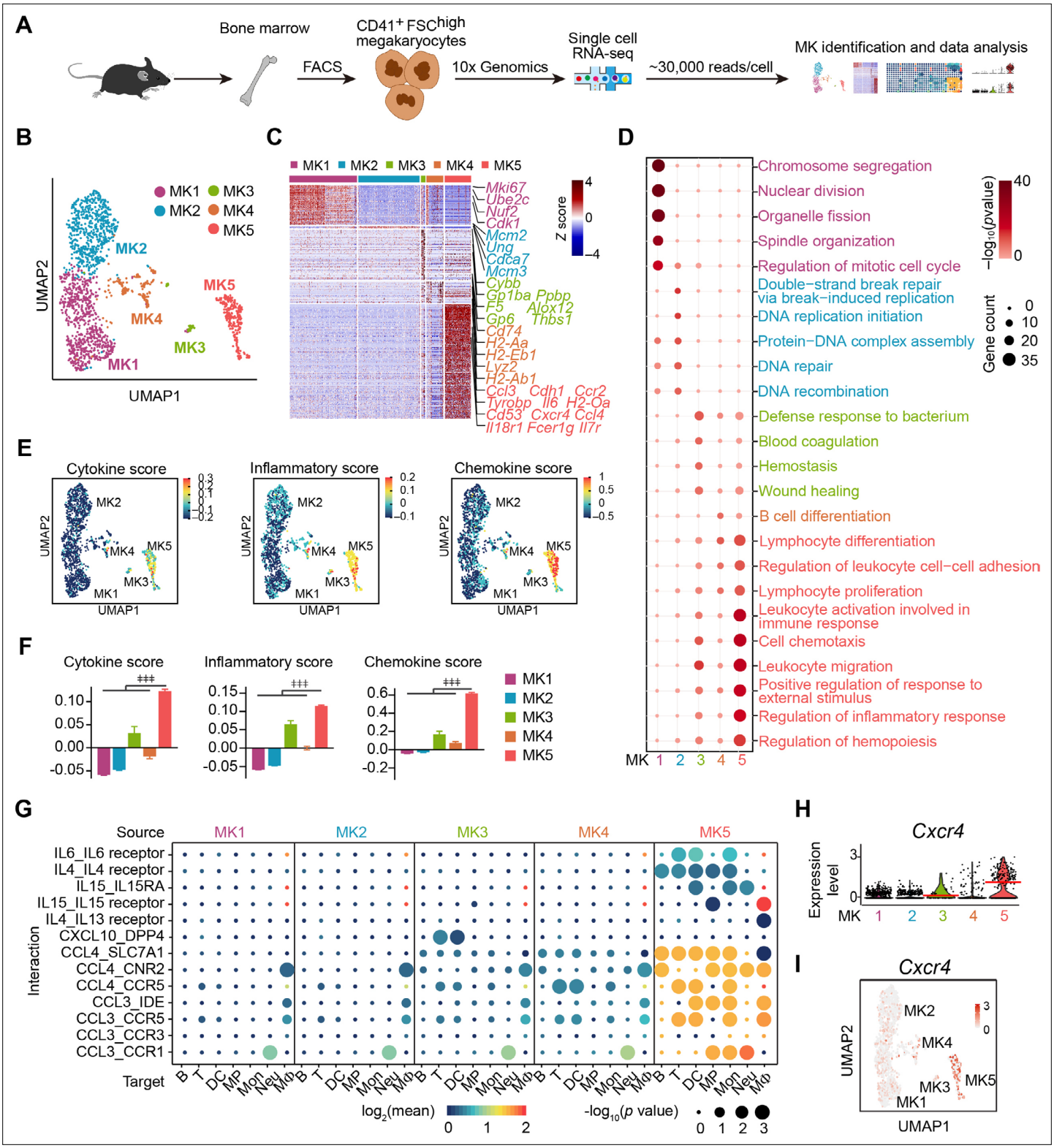

Figure 1. Single-cell atlas identifies an immune-modulatory subpopulation of MKs. (**A**) Schematic strategy for MK preparation, scRNA-seq and data analysis. (**B**) Clustering of 1712 bone marrow MKs. (**C**) Heatmap of signature gene expression in MK subpopulations (fold-change >1.5, p value <0.05) with exemplar genes listed on the right (top, color-coded by subpopulations). Columns denote cells; rows denote genes. Z score, row-scaled expression of the signature genes in each subpopulation. (**D**) Gene Ontology (GO) analysis of signature genes (fold-change >1.5, p value <0.05) for each MK subpopulations. GO terms selected with Benjamini–Hochberg-corrected p values <0.05 and colored by $-\log_{10}$(p value). Bubble size indicates the

Figure 1 continued on next page

Figure 1 continued

enriched gene number of each term. (**E–F**) UMAP visualization (**E**) and statistical analysis (**F**) of cytokine score (left), inflammatory score (middle) and chemokine score (right) in MK1 to 5. (**G**) Dotplots of significant cytokine ligand (source) -receptor (target) interactions between MKs and immune cells discovered. The color indicates the means of the receptor-ligand pairs between two cell types and bubble size indicates p values. Mon, monocytes; MΦ, macrophages (***Dong et al., 2020***); DC, dendritic cells; Neu, neutrophils; MP, myeloid progenitors; T, T cells; B, B cells. (**H–I**) Violin plot (**H**) and feature plot (**I**) of selected signature genes of MK5. Red lines in (**H**) indicate the median gene expression. Repeated-measures one-way ANOVA followed by Dunnett's test for multiple comparisons in (**F**), # <0.01, ## p<0.001.

The online version of this article includes the following source data and figure supplement(s) for figure 1:

Source data 1. Signature genes of MK1 to MK5.

Source data 2. The means and p value of the average expression level of interacting molecule 1 in cluster 1 and interacting molecule 2 in cluster 2 by CellPhoneDB.

Figure supplement 1. Cell isolation, quality control and annotation of scRNA-seq data.

Figure supplement 2. Cell type identification by alignment with published scRNA-seq data.

Figure supplement 3. Identification of MK subpopulations.

Figure supplement 4. Enriched genes in MK1 to 4 and MK5.

Figure supplement 5. MK5 interacts with immune cells and express signature genes of immune MKs.

Figure supplement 6. Polyploidy, platelet generation ability and cell size of CXCR4^{low} and CXCR4^{high} MKs.

expressed signature genes in recently reported inflammatory-related MKs (*Cd53*, *Lsp1*, *Anxa1*, *Spi*) (***Sun et al., 2021***) and immune MKs (*Ccl3*, *Cd52*, *Selplg*, *Sell*, *Adam8*) (***Liu et al., 2021***; ***Figure 1—figure supplement 5B***). We also noticed that MK5 highly expressed *Cxcr4* than other MK subpopulations (***Figure 1H,I***), although most MKs express CXCR4 (***Hamada et al., 1998***; ***Figure 1—figure supplement 6A***). To confirm this, we found that CXCR4^{high} MKs expressed MK markers (***Figure 1—figure supplement 6B***), were mainly polyploid cells (***Figure 1—figure supplement 6C***), and had platelet generation ability (***Figure 1—figure supplement 6D***), although they have relatively low polyploidy (***Figure 1—figure supplement 6E***) and smaller cell size (***Figure 1—figure supplement 6F-H***). CXCR4^{high} MKs generated platelets in lower efficiencies compared to CXCR4^{low} MKs (***Figure 1—figure supplement 6D***), suggesting CXCR4^{high} MKs might be specialized for immune functions. Overall, using scRNA-seq, we identified an MK subpopulation that exhibited both MK-specific and immune transcriptional characteristics.

CXCR4^{high} MKs enhance myeloid cell mobility and bacterial phagocytosis

As MK5 enriched genes involved in myeloid cell activation (***Figure 1—figure supplement 4E***) and myeloid cell interactions (***Figure 1G***, ***Figure 1—figure supplement 5A***), we further explored the role of CXCR4^{high} MKs, which enriched MK5, in regulating myeloid immune cells, in regulating the innate immunity function of myeloid cells against pathogens. We challenged mice with *Listeria* (*L.*) *monocytogenes*, a Gram-positive facultative intracellular bacterium (***Bishop and Hinrichs, 1987***; ***Edelson and Unanue, 2000***), which induce myelopoiesis (***Eash et al., 2009***; ***Figure 2—figure supplement 1A, B***). Interestingly, we noticed that CXCR4^{high} MKs were more dramatically associated with myeloid cells in the bone marrow of mice 3 days after *L. monocytogenes* infection, which was a significant increase than the association between myeloid cells and CXCR4^{low} MKs or the association between randomly placed myeloid cells and CXCR4^{high} MKs (***Figure 2A,B***). The myeloid cell-CXCR4^{high} MK association (mean distance 15.36 μm) was significantly closer than the myeloid cell-CXCR4^{low} MKs association (***Figure 2C***; mean distance 25.62 μm, $p=7.0 \times 10^{-4}$ by KS test), and the association between randomly placed myeloid cells and CXCR4^{high} MKs [35.37 μm, p (μ<15.36)$=1.8 \times 10^{-10}$] in the bone marrow of mice 3 days after *L. monocytogenes* infection. Whereas the observed mean distance of myeloid cells to CXCR4^{low} MKs (25.62 μm) is not different from random simulations [27.76 μm, p (μ<25.62)=0.14] (***Figure 2C***). This suggested that the increased association between myeloid cell-CXCR4^{high} MK may not be due to the infection-induced expansion of myeloid cells. Furthermore, we did not observe a significant association between myeloid cells and MKs during homeostasis (***Figure 2—figure supplement 1C,D***). We also noticed that bone marrow myeloid cells were preferably adjacent to the CXCR4^{high} MK-blood vessel intersection in mice 3 days after *L. monocytogenes*

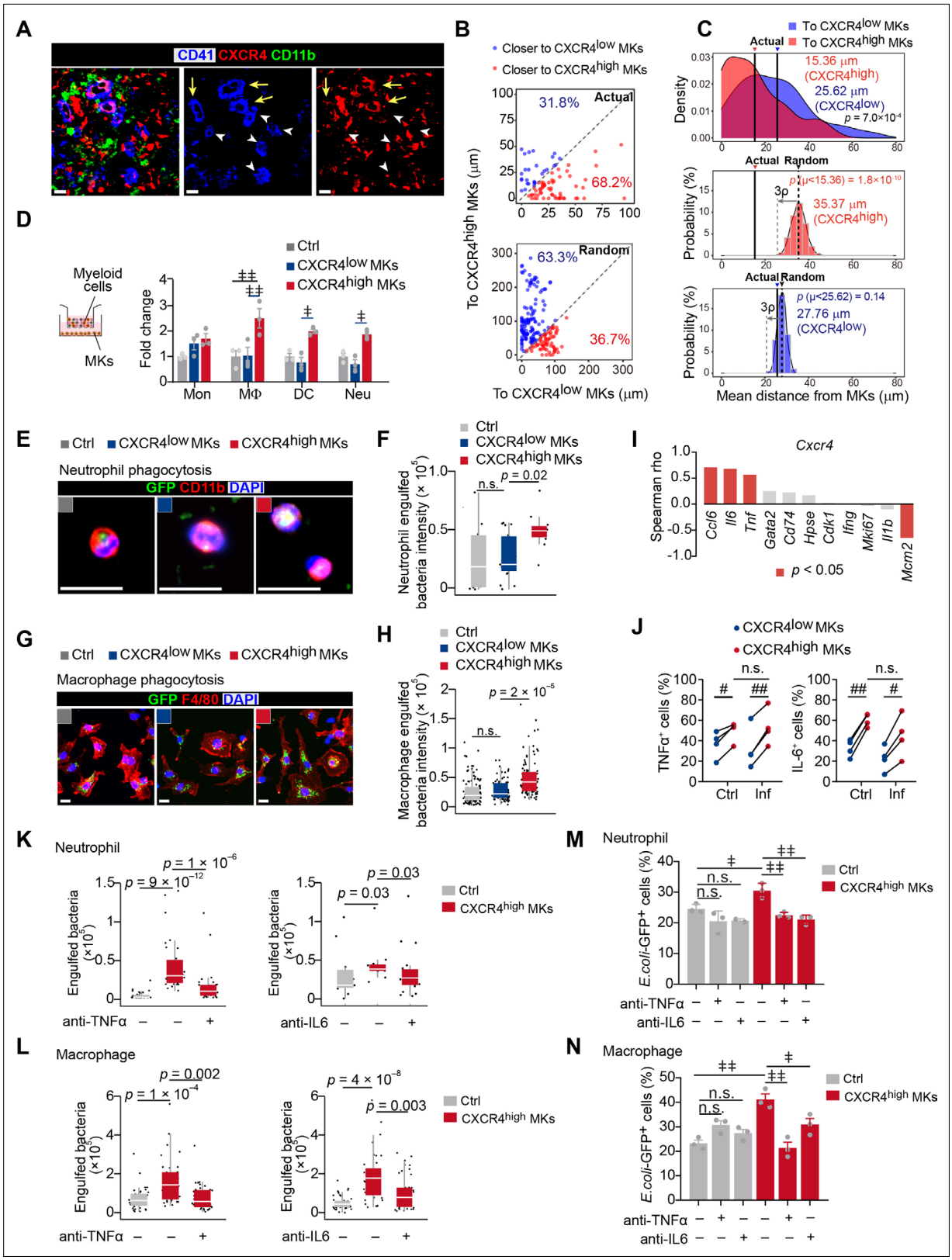

Figure 2. CXCR4^{high} MKs enhance myeloid cell mobility and bacteria phagocytosis. (**A**) Distribution of myeloid cells to CXCR4^{low} or CXCR4^{high} MKs 3 days after *L. monocytogenes* infection. Representative images of MKs (blue), CXCR4 (red), and myeloid cells (green) in mouse bone marrow. Yellow arrows indicate CXCR4^{high} MKs and white arrowheads indicate CXCR4^{low} MKs. (**B–C**) Distance (**B**) and mean distance (**C**) of actual or randomly positioned myeloid cells to the closest CXCR4^{low} and CXR4^{high} MKs 3 days after *L. monocytogenes* infection. (**D**) Numbers of transmigrated myeloid

Figure 2 continued on next page

Figure 2 continued

cells normalized to Ctrl (without MKs in the lower chambers) as indicated by transwell assays. Mon, monocytes; MΦ, macrophages; DC, dendritic cells; Neu, neutrophils. (**E–F**) Representative images (**E**) and quantification (**F**) of neutrophil phagocytosis capacity with or without MK co-culture as indicated. CD11b, red; *E. coli*, green; DAPI, blue. Ctrl, neutrophil without MK co-culture. (**G–H**) Representative images (**G**) and quantification (**H**) of macrophage phagocytosis capacity with or without MK co-culture as indicated. F4/80, red; *E. coli*, green; DAPI, blue. Ctrl, macrophage without MK co-culture. (**I**) Spearman correlation analysis between expression profiles of *Cxcr4* and feature genes in MK subpopulations. (**J**) Quantification of TNFα^{+} and IL-6^{+} cells in CXCR4^{low} MKs and CXCR4^{high} MKs from control mice or mice 3 days after *L. monocytogenes* infection. (**K–L**) Quantification of neutrophil (**K**) and macrophage (**L**) phagocytosis with or without CXCR4^{high} MK co-culture in the absence or presence of anti-TNFα or anti-IL-6 neutralizing antibodies. (**M–N**) Quantification of the phagocytosis abilities by neutrophils (**M**) and macrophages (**N**) with or without CXCR4^{low} MK or CXCR4^{high} MK co-culture in the absence or presence of anti-TNFα or anti-IL-6 neutralizing antibodies by flow cytometry. Ctrl, neutrophils (**M**) or macrophages (**N**) without MKs co-culture. Scale bars, 20 μm (**A, E, G**). Data represent mean ± s.e.m (**D**) and boxplots show medians, first and third quartiles (**F, H, K–L**). Repeated-measures one-way ANOVA followed by Dunnett's test for multiple comparisons in (**D, M, N**), ǂ p<0.05, # p<0.01, n.s., not significant. A two-sample KS test was performed to assess statistically significant (**C, F, H, K, L**), n.s., not significant. Paired Student's *t*-test was performed to assess statistical significance (**J**), # p<0.05, ## p<0.01, n.s., not significant.

The online version of this article includes the following source data and figure supplement(s) for figure 2:

Source data 1. Distance of actual myeloid cells to the closest CXCR4^{low} and CXR4^{high} MKs 3 days after *L. monocytogenes* infection.

Source data 2. Distance of randomly positioned myeloid cells to the closest CXCR4^{low} and CXR4^{high} MKs 3 days after *L. monocytogenes* infection.

Source data 3. Mean distance of randomly positioned myeloid cells to the closest CXCR4^{low} and CXR4^{high} MKs 3 days after *L. monocytogenes* infection from 500 times simulations.

Figure supplement 1. *L. monocytogenes* promote myelopoiesis and the association of myeloid cells and the CXCR4^{high} MK-blood vessel intersection.

Figure supplement 2. CXCR4^{high} MKs promote myeloid cell phagocytosis and produce TNFα and IL-6.

infection (***Figure 2—figure supplement 1E,F***). These observations indicated that CXCR4^{high} MKs might regulate myeloid cells upon bacterial infection.

To explore how CXCR4^{high} MKs regulate myeloid cells, we interestingly found that CXCR4^{high} MKs, but not CXCR4^{low} MKs, effectively promoted myeloid cell mobilization in our transwell assays (***Figure 2D***). Furthermore, we asked whether CXCR4^{high} MKs regulate myeloid cell function against pathogens. To this aim, we incubated purified CXCR4^{low} MKs and CXCR4^{high} MKs with neutrophils or macrophages for bacterial phagocytosis analysis. We found that CXCR4^{high} MKs, but not CXCR4^{low} MKs, efficiently enhanced the bacterial phagocytosis of neutrophils and macrophages (***Figure 2E–H***; ***Figure 2—figure supplement 2A,B***).

Our scRNA-seq also exhibited that the high expression of *Cxcr4* was positively correlated with immune cell-stimulating cytokines, such as *Ccl6*, *Tnf*, and *Il6* (***Li et al., 2018***; ***Rothe et al., 1993***; ***Shapouri-Moghaddam et al., 2018***) in MKs (***Figure 2I***). In line with this, CXCR4^{high} MKs had higher TNFα and IL-6 protein levels than CXCR4^{low} MKs (***Figure 2J***; ***Figure 2—figure supplement 2C,D***). The TNFα and IL-6 levels in CXCR4^{high} MKs were comparable to macrophages from mice 3 days after *L. monocytogenes* infection (***Figure 2—figure supplement 2E***), which are known as the primary cellular source of TNFα and IL-6 upon infection (***Shapouri-Moghaddam et al., 2018***). These observations suggested that CXCR4^{high} MKs might stimulate myeloid cell phagocytosis by producing TNFα and IL-6. Indeed, anti-TNFα and anti-IL-6 blocking antibodies compromised the role of CXCR4^{high} MKs in stimulating bacterial phagocytosis of neutrophils and macrophages (***Figure 2K–N***).

CXCR4^{high} MKs stimulate host-defense immunity against bacterial pathogens

To explore the in vivo role of MKs upon *L. monocytogenes* infection in mice, we employed *Pf4^{Cre}*; *Rosa26$^{fs\text{-}iDTR}$* mice, in which MKs were rendered sensitive to diphtheria toxin (DT) (***Zhao et al., 2014***; ***Figure 3A and B***). MK ablation increased the number of hematopoietic stem and progenitor cells and myelopoiesis in the bone marrow upon infection (***Figure 3—figure supplement 1A-D***). Notably, MK ablation dramatically increased the bacterial burdens in the liver and spleen 3 days after *L. monocytogenes* infection (***Figure 3C***). We also found that MK ablation reduced the number of myeloid cells, including monocytes, macrophages, dendritic cells (DCs), and neutrophils, in the liver and spleen (***Figure 3D,E***; ***Figure 3—figure supplement 1E,F***), suggesting the role of MKs in promoting myeloid cells against pathogens. We further investigated whether MKs regulate adaptative immunity against pathogen infection. Interestingly, we noticed that CXCR4^{high} MKs were able to phagocytose bacteria and presented the ovalbumin (OVA) antigens on their surface via MHC-I (***Figure 3F,G***). Furthermore,

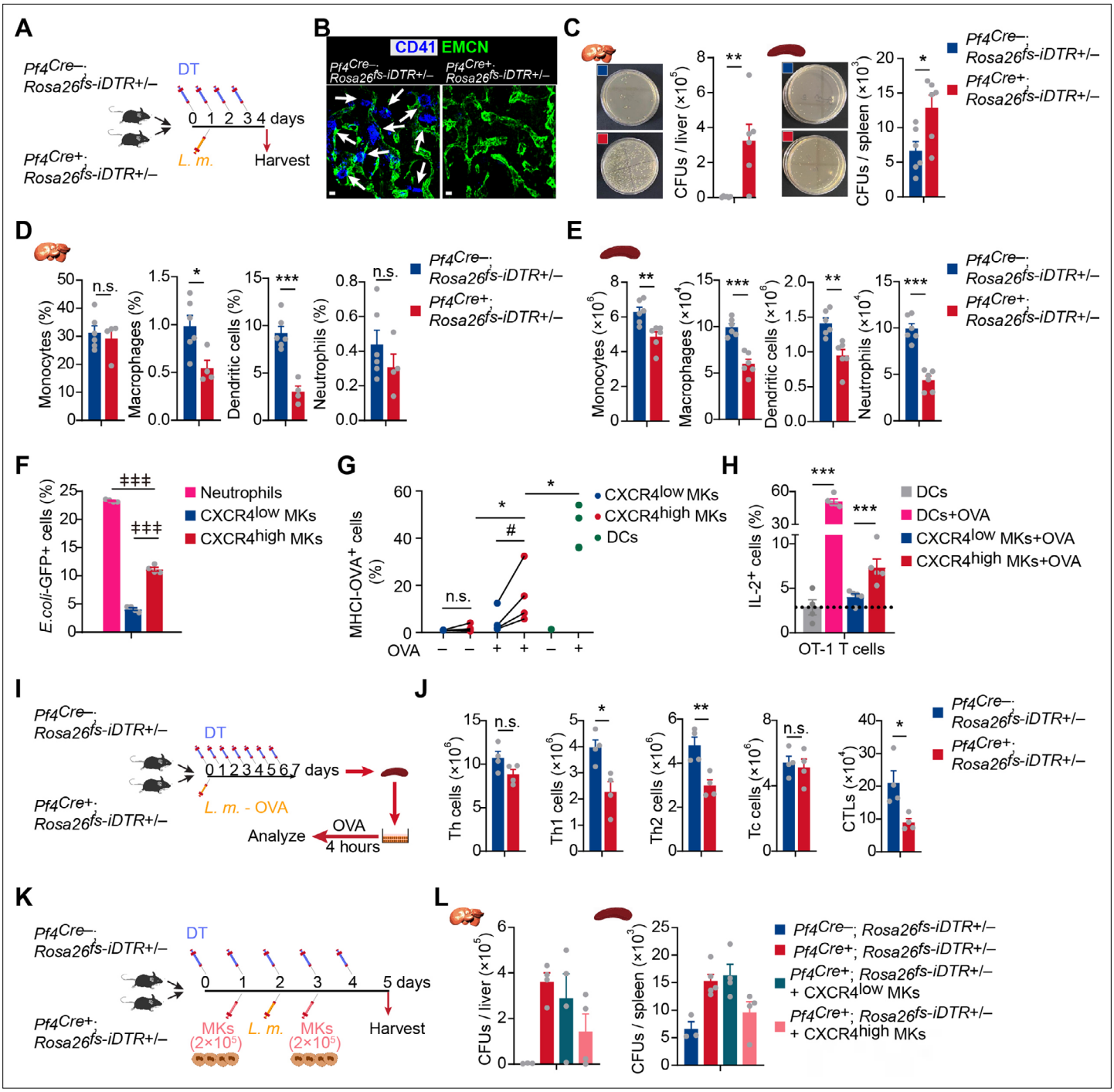

Figure 3. CXCR4^{high} MKs stimulate host-defense immunity against bacterial pathogens. (**A**) Schema for diphtheria toxin (DT) and *L. monocytogenes* administration used for the experiments shown in (**B–E**). (**B**) Representative images of MKs (blue, indicated by arrows) and vascular endothelial cells (green) in the bone marrow of mice after four daily DT treatments. (**C**) Bacterial burdens in the liver and spleen of *Pf4*^{Cre}; *Rosa26*$^{fs\text{-}iDTR}$ mice 3 days after *L. monocytogenes* (*L.m.*) infection with four-time DT injections. (**D–E**) Myeloid cells in the liver (**D**) and spleen (**E**) of *Pf4*^{Cre}; *Rosa26*$^{fs\text{-}iDTR}$ mice 3 days after *L. monocytogenes* (*L.m.*) infection with four-time DT injections. (**F**) Quantification of bacterial phagocytosis capacities of neutrophils, CXCR4^{low} MKs and CXCR4^{high} MKs. (**G**) Quantification of MHCI-OVA levels on CXCR4^{low} MKs, CXCR4^{high} MKs and bone-marrow-derived dendritic cells (DCs) upon a pulse of 24 hr with or without OVA. (**H**) Quantification of activated OT-I CD8^{+} T cells after co-culture with bone-marrow-derived DCs, OVA-pulsed bone-marrow-derived DCs, CXCR4^{low} MKs, or CXCR4^{high} MKs. (**I**) Schema for antigen-specific T cell activation assay shown in (**J**). (**J**) Splenocytes from control or MK ablated mice 7 days after *L. monocytogenes*-OVA$_{257\text{-}264}$ infection and seven DT injections were stimulated with OVA peptide in vitro for 4 hr, and antigen-specific activated T cells were quantified (n=4 mice). *L.m.*-OVA, *L. monocytogenes*-OVA$_{257\text{-}264}$. (**K**) Schema for DT, *L. monocytogenes* administration, MK transfusing and bacterial burden determination shown in (**L**). (**L**) Bacterial burdens in the liver and spleen of *Pf4*^{Cre}; *Rosa26*$^{fs\text{-}iDTR}$ mice without or with

Figure 3 continued on next page

Figure 3 continued

CXCR4^{low} or CXCR4^{high} MK transfused. Scale bars, 20μm. Data represent mean ± s.e.m. Repeated-measures one-way ANOVA followed by Dunnett's test for multiple comparisons in (**F**), ## p<0.001. Paired Student's *t*-test was performed to assess statistical significance (**G**), # p<0.05, n.s., not significant. Two-tailed Student's *t*-test was performed to assess statistical significance except (**F**), * p<0.05, ** p<0.01, *** p<0.001, n.s., not significant.

The online version of this article includes the following figure supplement(s) for figure 3:

Figure supplement 1. MK ablation influenced HSC and myeloid cell numbers.

Figure supplement 2. CXCR4^{high} MKs induced B3Z T cell activation.

OVA antigens presented by CXCR4^{high} MKs activated OT-I CD8^{+} T cells (***Figure 3H***) and B3Z T cells (***Figure 3—figure supplement 2***), a T cell hybridoma which expresses TCR that specifically recognizes OVA (***Karttunen et al., 1992***). We challenged *Pf4^{Cre}; Rosa26$^{fs\text{-}iDTR}$* mice with OVA-expressing recombinant microbe (*L. monocytogenes*-OVA). Seven days after *L. monocytogenes*-OVA infection, splenocytes from control or MK ablated mice were re-stimulated with OVA peptide in vitro to assess OVA-specific T cell activation (***Figure 3I***). Notably, MK ablation dramatically reduced the number of CD4^{+} IFNγ^{+} Th1, CD4^{+} IL4^{+} Th2, and CD8^{+} cytotoxic T lymphocytes but did not impact the total number of CD4^{+} T cells and CD8^{+} T cells (***Figure 3J***). These observations demonstrated that MKs regulate host-defense immunity against *L. monocytogenes* infection. To explore whether CXCR4^{high} MKs contribute to the immune response against bacterial pathogens, we infused the purified CXCR4^{high} MKs and CXCR4^{low} MKs into MK ablation mice during *L. monocytogenes* infection (***Figure 3K***). Notably, we found that the infusion with CXCR4^{high} MKs, but not CXCR4^{low} MKs, partially rescued the bacterial clearance defect in MK ablation mice (***Figure 3L***). This is potentially due to the reduced platelets known for regulating immune responses (***Semple et al., 2011***).

Bacterial infection stimulates the migration of CXCR4^{high} MKs

High *Cxcr4* expression indicated that CXCR4^{high} MKs might migrate between the bone marrow microenvironment and circulation in response to infection (***Suraneni et al., 2018***). In line with this, our spatial distribution analysis showed that ~80% of MKs directly contacted blood vessels 3 days after *L. monocytogenes* infection, which was much higher than in control mice (~40%) (***Figure 4A,B***; ***Figure 4—figure supplement 1A***). Furthermore, more CXCR4^{high} MKs, with small cell sizes (***Figure 1—figure supplement 6F-H***), were tightly associated with blood vessels and trapped in the sinusoid than CXCR4^{low} MKs 3 days after *L. monocytogenes* infection (***Figure 4C,D***). However, *L. monocytogenes* infection did not influence the association between MKs and HSCs (***Figure 4A,E***), albeit the critical role of perivascular MKs in maintaining HSC quiescence (***Bruns et al., 2014***; ***Itkin et al., 2016***; ***Zhao et al., 2014***) and the dramatic HSC activation upon infection (***Figure 4—figure supplement 1B***).

To further explore the dynamic migration of MKs upon pathogen infection, we adapted an ex vivo real-time imaging method to trace MK migration in the bone marrow (***Xie et al., 2009***). Using *Pf4^{Cre}; Rosa26$^{fs\text{-}tdTomato}$* mice and ex vivo live imaging approach, we observed that small tdTomato^{+} MKs rapidly migrated into sinusoids without rupture or platelet release upon infection (***Figure 4F***, ***Figure 4—video 1***). In contrast, MKs with large sizes showed much slower migration (***Figure 4—video 1***). Additionally, CXCR4^{high} MKs were decreased in the bone marrow 3 days after *L. monocytogenes* infection but with a similar proliferation and apoptosis rate compared to CXCR4^{low} MKs (***Figure 4G***; ***Figure 4—figure supplement 1C-F***), indicating CXCR4^{high} MKs might migrate out of bone marrow. Consistent with this, the frequency of MK5, which enriched CXCR4^{high} MKs, decreased in bone marrow after *L. monocytogenes* infection in our single-cell atlas (***Figure 4—figure supplement 2***). Furthermore, we found that *L. monocytogenes* infection decreased the expression of CXCL12, the ligand of CXCR4 (***Sugiyama et al., 2006***), in bone marrow but increased CXCL12 expression in the lung, liver, and spleen (***Figure 4—figure supplement 3***), suggesting that the distinguished CXCL12 levels between tissues might drive the migration of CXCR4^{high} MKs between tissues. In line with this, CXCR4^{high} MKs were increased in the peripheral blood and organs, including the liver, spleen, and lung 3 days after *L. monocytogenes* infection without an alternation of cell cycle and apoptosis, whereas CXCR4^{low} MKs did not differ except for a slight increase in the liver (***Figure 4G***; ***Figure 4—figure supplement 4A-C***). Moreover, inflammatory stresses, such as IFNγ and Lipopolysaccharides (LPS), or *L. monocytogenes* treatment did not increase CXCR4 expression in CXCR4^{low} MKs (***Figure 4H***; ***Figure 4—figure supplement 4D***).

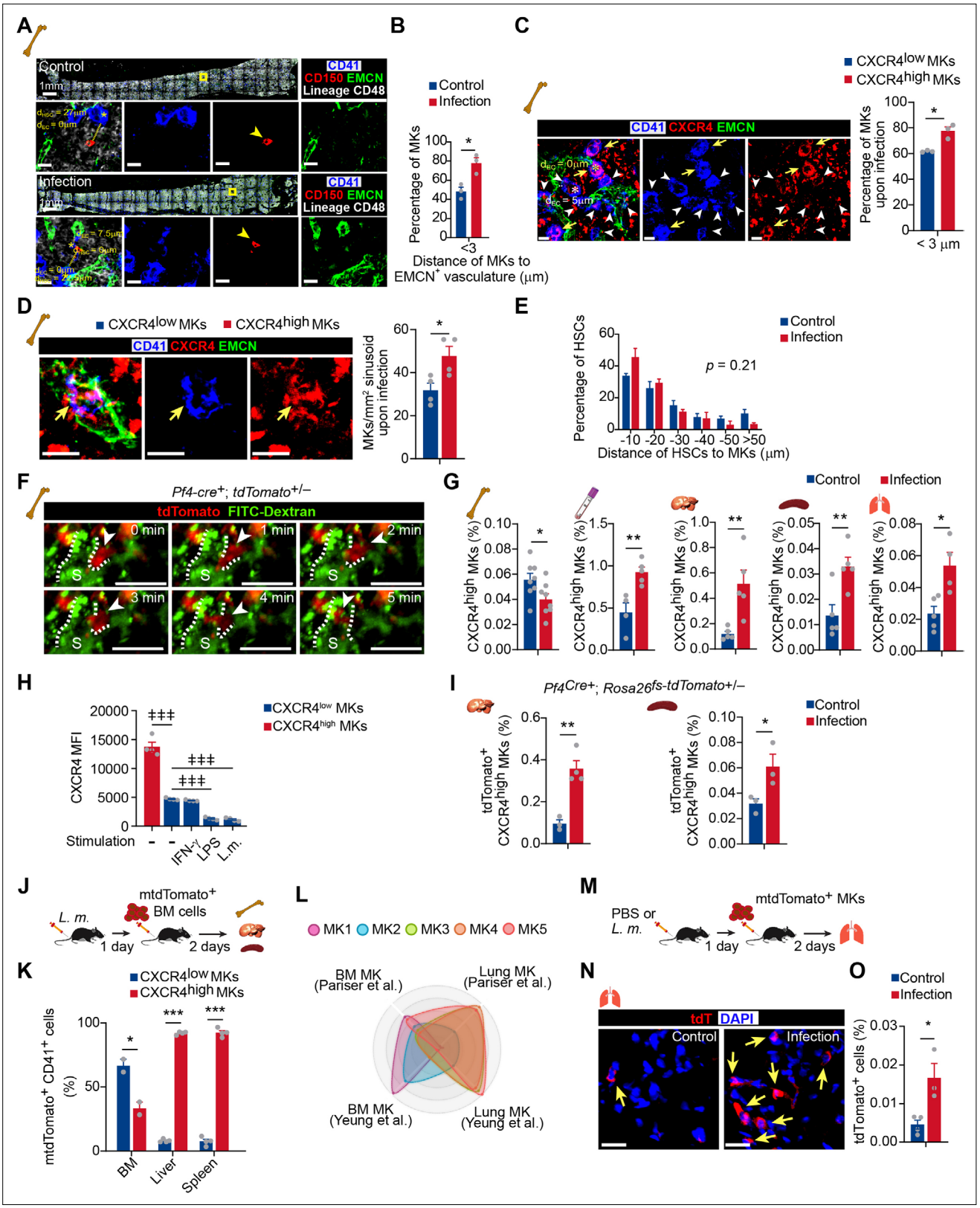

Figure 4. Bacterial infection stimulates the migration of CXCR4^{high} MKs. (**A**) Representative image of CD41 (blue), CD150 (red), EMCN (green), and lineage cells (white) in bone marrow from control mice or mice at 3 days after *L. monocytogenes* infection. d_{HSC} and d_{EC} indicate the distance between the MK (blue, marked with an asterisk) and the closest HSC (red), endothelial cell (green), respectively. Yellow boxes indicate the locations of the magnified images. Arrowheads indicate HSCs. EMCN, endomucin; EC, endothelial cell. (**B**) Comparison of the distance between MKs to Ecs (n=119

Figure 4 continued on next page

Figure 4 continued

control and 103 infected MKs) in the bone marrow of control mice or mice at 3 days after *L. monocytogenes* infection. (**C**) Comparison of the distance between CXCR4^{low} or CXCR4^{high} MKs and endothelial cells (Ecs) in the bone marrow of mice 3 days after *L. monocytogenes* infection (n=68 CXCR4^{low} and 78 CXCR4^{high} MKs). CD41 (blue), CXCR4 (red), and EMCN (green). Yellow arrows indicate CXCR4^{high} MKs, while white arrowheads indicate CXCR4^{low} MKs. (**D**) Representative immunofluorescent staining images (left) and quantification (right) of CXCR4 (red) labeled MKs (blue) egressed into sinusoids (green) upon infection (n=46 CXCR4^{low} MKs and 69 CXCR4^{high} MKs in 4 biological replicates). Yellow arrows indicate CXCR4^{high} MKs. (**E**) Comparison of the distance between HSCs to MKs (n=96 control and 127 infected HSCs, p=0.21 by two-sample KS test) in the bone marrow of control mice or mice at 3 days after *L. monocytogenes* infection. (**F**) Visualization of MK migration (red, arrowhead) into sinusoids (green) by live imaging in the bone marrow of *Pf4^{Cre+}*; *Rosa26$^{fs\text{-}tdTomato+/-}$* mice 24 hr after *L. monocytogenes* infection (Movie S1). 'S' indicates sinusoid and dashed lines demarcate the border of sinusoids. (**G**) Quantification of CXCR4^{high} MKs in bone marrow, peripheral blood, liver, spleen, and lung of control mice and mice 3 days after *L. monocytogenes* infection. (**H**) Quantification of CXCR4 levels on CXCR4^{low} MKs treated with IFN-γ, LPS or *L. monocytogenes* for 4 hr compared to CXCR4^{high} MKs. (**I**) Quantification of tdTomato^{+} CXCR4^{high} MKs in the liver and spleen from control mice or mice 3 days after *L. monocytogenes* infection by flow cytometry. (**J**) Schema of mtdTomato^{+} bone marrow (from *R26R^{mTmG}* mice) cell perfusion in control and *L. monocytogenes* infected recipients. (**K**) The percentage of CXCR4^{high} mtdTomato^{+} MKs and CXCR4^{low} mtdTomato^{+} MKs in bone marrow, liver, and spleen of control or infected recipients were analyzed 2 days after mtdTomato^{+} bone marrow cells were perfused. (**L**) Radar chart showing transcriptomic similarities of bone marrow MK subpopulations with reported BM and lung MK datasets (***Pariser et al., 2021***; ***Yeung et al., 2020***). (**M**) Schema for transfer experiments using tdTomato^{+} MKs from *Pf4^{Cre+}*; *Rosa26$^{fs\text{-}tdTomato+/-}$* mice into control recipients or recipients 1 day following *L. monocytogenes* infection. (**N–O**) Representative images (**N**) and quantification by flow cytometry (**O**) of tdTomato^{+} MKs in the lung of control or infected recipients 2 days after cell perfusion (n=3 mice). Arrows indicate tdTomato^{+} MKs in the lung. Scale bars without indicated, 20 μm. Data represent mean ± s.e.m. A two-sample KS test was performed to assess statistical significance in (**E**). Repeated-measures one-way ANOVA followed by Dunnett's test for multiple comparisons in (**H**), # p<0.01, ## p<0.001. Two-tailed Student's *t*-test was performed to assess statistical significance except (**E, H**), * p<0.05, ** p<0.01, *** p<0.001, n.s., not significant.

The online version of this article includes the following video, source data, and figure supplement(s) for figure 4:

Source data 1. Distance of HSCs to MKs in the bone marrow from control mice or mice 3 days after *L. monocytogenes* infection.

Figure supplement 1. The effects of association of MKs and blood vessels, HSC activation, and MK numbers in bone marrow upon bacterial infection.

Figure supplement 2. scRNA-seq of MKs from mice upon bacterial infection.

Figure supplement 3. CXCL12 expression upon bacterial infection.

Figure supplement 4. Cell cycle and apoptosis of CXCR4^{high} MKs, and CXCR4^{low} MK numbers in different organs upon bacterial infection.

Figure supplement 5. Comparison of immune gene expression in MK5 and lung MKs from control mice or mice upon bacterial infection.

Figure supplement 6. Intravascular and extravascular tdTomato^{+} MKs in the lung after MK perfusion.

Figure 4—video 1. MK migration traced by ex vivo live imaging.
https://elifesciences.org/articles/78662/figures#fig4video1

To further explore how MKs migrate between organs during bacterial infection in vivo, we employed *Pf4^{Cre}; Rosa26$^{fs\text{-}tdTomato}$, and Pf4^{Cre}; cell membrane-localized tdTomato cell membrane-localized EGFP* (*Rosa26$^{fs\text{-}mTmG}$*) mice in which Tomato or cell membrane-localized EGFP (mGFP) were exclusively expressed in MK lineage (***Tiedt et al., 2007***). mGFP expressing MKs or Tomato expressing CXCR4^{high} MKs were increased in the liver and spleen 3 days after *L. monocytogenes* infection (***Figure 4I***; ***Figure 4—figure supplement 4E-H***), whereas Tomato expressing CXCR4^{low} MKs did not change (***Figure 4—figure supplement 4I***). To further confirm the tissue infiltration of MKs upon infection, we intravenously injected membrane-localized tdTomato (mTomato) expressing bone marrow cells from *Rosa26R$^{fs\text{-}mTmG}$* mice into control recipients or recipients infected with *L. monocytogenes* 1 day before mTomato^{+} cell perfusion (***Figure 4J***). We found that 2 days after mTomato^{+} cell perfusion, engrafted mTomato^{+} CXCR4^{high} MKs more efficiently infiltrated into the liver (92.1%) and spleen (92.5%); by contrast, most mTomato^{+} CXCR4^{low} MKs (66.7%) migrated to the bone marrow (***Figure 4K***).

As the lung is an important site for platelet generation (***Lefrançais et al., 2017***), we aligned our MK sc-RNAseq data with lung MKs (***Pariser et al., 2021***; ***Yeung et al., 2020***), and found that MK5, MK4, and MK3 showed similar gene profiles with lung MKs (***Figure 4L***). Moreover, MK5 enriched more inflammatory pathway genes, antigen processing, and presentation pathway after *L. monocytogenes* infection, which enabled MK5 to achieve a more similar transcriptional profile as the lung MKs than normal MK5 (***Figure 4—figure supplement 5***). Interestingly, we found that engrafted Tomato^{+} MKs (from *Pf4^{Cre}; Rosa26$^{fs\text{-}tdTomato}$* mice) more efficiently infiltrated the lungs in the infected recipients as extravascular MKs than in the control recipients (***Figure 4M–O*** and ***Figure 4—figure supplement 6***).

Acute inflammation-induced emergency megakaryopoiesis generates CXCR4^{high} MKs upon infection

Infection-induced emergency megakaryopoiesis compensates the platelet consumption (**Verschoor et al., 2011**). Consistently, we observed that MKs were ruptured in the bone marrow 3 days after *L. monocytogenes* infection to recover the reduced platelets post-*L. monocytogenes* infection (**Couldwell and Machlus, 2019**; **Nishimura et al., 2015**; **Figure 5A–C**). However, CXCR4^{high} MKs were increased at 18 hr after *L. monocytogenes* infection and substantially declined at 72 hr in bone marrow, whereas CXCR4^{low} MKs remained unchanged upon infection (**Figure 5D**). As MK-committed HSCs drive infection-induced emergency megakaryopoiesis (**Haas et al., 2015**), we asked whether emergency megakaryopoiesis also generates CXCR4^{high} MKs to participate in the host-defense response. To this aim, we employed *Scl^{CreER}; Rosa26$^{fs\text{-}tdTomato}$* mice (**Göthert et al., 2005**) to monitor the HSPC derived emergency megakaryopoiesis upon bacterial infection. Eighteen hours after tamoxifen recombining Tomato in HSPCs and *L. monocytogenes* infection (**Figure 5E**), we observed that Tomato^{+} HSPCs derived Tomato^{+} CXCR4^{high} MKs rapidly increased in the bone marrow, similar to the platelet-generating MKs (tdTomato^{+} CXCR4^{low} MKs) (**Figure 5F**), without a noticeable rise of hematopoietic progenitors (**Figure 5G**). Overall, our observations indicated that CXCR4^{high} MKs might be generated by emergency megakaryopoiesis to stimulate pathogen defense.

Discussion

MKs participate in megakaryocyte maturation, platelet activation, and potentially influence neutrophils and the adaptive immune cells (**Cunin and Nigrovic, 2019**). Accordingly, MKs prevent the spread of dengue virus infection by enhancing the type 1 interferons pathway in murine and clinical biospecimens (**Campbell et al., 2019**) and contribute to cytokine storms in severe COVID-19 patients (**Bernardes et al., 2020**; **Ren et al., 2021**; **Stephenson et al., 2021**). MKs were reported to express multiple inflammation receptors, such as Fcγ receptors (**Markovic et al., 1995**), Toll-like receptors (**Beaulieu et al., 2011**; **Ward et al., 2005**), interleukin receptors (**Navarro et al., 1991**; **Yang et al., 2000**), and IFN receptors (**Negrotto et al., 2011**), which might enable MKs to receive inflammation signals and express cytokines. Recent scRNA-seq studies suggested the existence of MK subpopulations for inflammation responses (**Liu et al., 2021**; **Pariser et al., 2021**; **Sun et al., 2021**; **Wang et al., 2021a**). Here, we identified that MK5 has both MK and immune cell characteristics for platelet generation and immune responses. More importantly, we demonstrated that CXCR4^{high} MKs recruited and stimulated innate myeloid cells by producing TNFα and IL-6, for bacterial phagocytosis. Furthermore, CXCR4^{high} MKs had the ability for antigen processing and antigen presentation capacity, which suggested that CXCR4^{high} MKs might contribute to the regulation of adaptive immune function. This is consistent with a previous observation that lung MKs are able to process and present antigens (**Pariser et al., 2021**). Our data suggested that CXCR4^{high} MKs might contribute to the regulation of adaptive immune function. However, as the distinction between CXCR4^{high} MKs and CXCR4^{low} MKs is not entirely objective, additional markers are warranted to further enrich CXCR4^{high} MKs.

We observed that MK ablation increased HSPCS and myeloid granulocyte/macrophage progenitor (GMP) in bone marrow under bacterial infection, which is consistent with 5-FU stress (**Hérault et al., 2017**). However, increased GMP only increased myeloid cells in the bone marrow but not in other organs, which further supported the role of CXCR4^{high} MKs in promoting the migration of myeloid cells. Normal HSC to MK development takes 11–12 days in humans and 4 days in mice; However, emergency megakaryopoiesis takes less than a day to generate MKs upon inflammation stress (**Couldwell and Machlus, 2019**; **Liu et al., 2021**; **Sun et al., 2021**; **Figure 5D**). Previously, researchers believed that emergency megakaryopoiesis mainly contributes to the replenishment of damaged platelets upon acute inflammation (**Haas et al., 2015**). We found that inflammation signals could not upregulate CXCR4 in CXCR4^{low} MKs in vitro, although we cannot entirely exclude the plasticity of MKs in vivo. Our data showed that CXCR4^{high} MKs might be generated from the emergency megakaryopoiesis, instead of CXCR4^{low} MKs, to facilitate host-defense responses against bacterial infection.

A recent report showed that the lung is a reservoir of MKs for platelet production (**Lefrançais et al., 2017**). Other works also indicate that lung MKs share a similar transcriptional profile with lung DCs and participate in pathogen infection (**Boilard and Machlus, 2021**; **Pariser et al., 2021**). However, the correspondence between MKs in the lung and bone marrow remains unexplored. Neonatal lung MKs

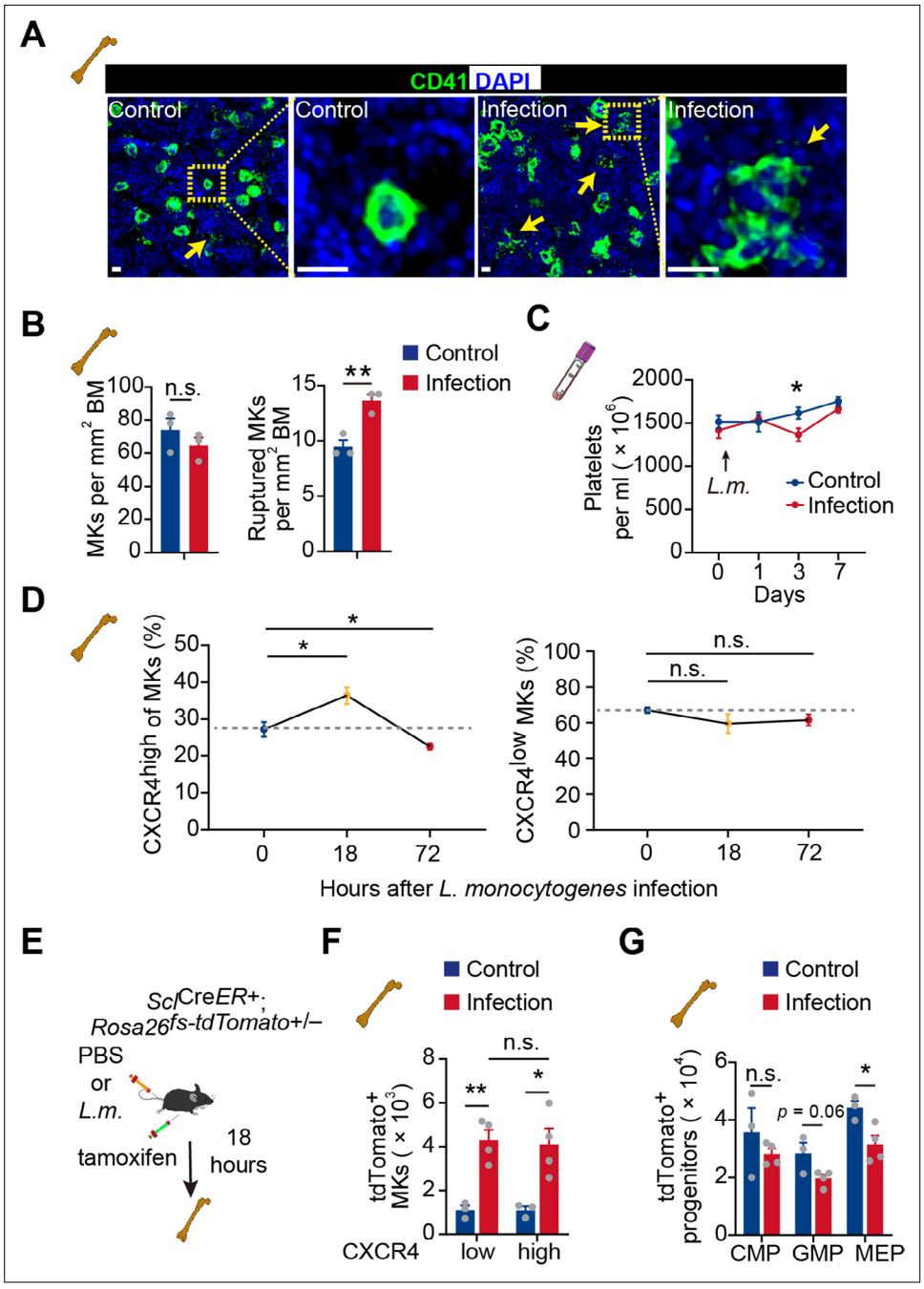

Figure 5. Acute inflammation induces emergency megakaryopoiesis of CXCR4^{high} MKs. (**A–B**) Representative images (**A**) and statistical analysis (**B**) of CD41 (green) and DAPI (blue) in bone marrow from control mice or mice 3 days after *L. monocytogenes* infection. Arrows indicate ruptured MKs, yellow boxes indicate the locations of the magnified images. (**C**) Platelets in peripheral blood in control mice or mice after *L. monocytogenes* infection on indicated days. (**D**) The dynamics percentage of CXCR4^{high} MKs (left) or CXCR4^{low} MKs (right) in the bone marrow of *L. monocytogenes*-challenged mice within 72 hr of infection. (**E**) Schema for HSC lineage tracing upon *L. monocytogenes* infection using *Scl*$^{CreER+}$; *Rosa26*$^{fs\text{-}tdTomato+/-}$ mice. (**F–G**) Cell numbers of tdTomato^{+} CXCR4^{low} MKs and tdTomato^{+} CXCR4^{high} MKs (**F**), and tdTomato^{+} progenitors (**G**) in the bone marrow of control and *L. monocytogenes* infected *Scl*$^{CreER+}$; *Rosa26*$^{fs\text{-}tdTomato+/-}$ recipients 18 hr after *L. monocytogenes* infection and tamoxifen administration. CMP, common myeloid progenitor; GMP, granulocyte-monocyte progenitor; MEP, megakaryocyte-erythroid progenitor. Scale bars, 20 μm. Data represent mean ± s.e.m. Two-tailed Student's *t*-test was performed to assess statistical significance, * p<0.05, ** p<0.01, n.s., not significant.

lack the immune molecules in adult lung MKs (***Pariser et al., 2021***), which indicates that lung MKs might have distinct developmental origins. Similarly, MKs are observed to egress and migrate to the pulmonary capillary under stresses (***Davis et al., 1997***). Our works suggested lung MKs might migrate from bone marrow upon infection challenges, although more detailed investigations are warranted in future studies.

Materials and methods

Key resources table

Reagent type (species) or resource	Designation	Source or reference	Identifiers	Additional information
Antibody	Anti-CD41a (mouse monoclonal)	eBioscience	Cat#17-0411-82 RRID:AB_1603237	FACS (1 µl per test)
Antibody	Anti-CXCR4 (mouse monoclonal)	eBioscience	Cat#53-9991-80 RRID:AB_953573	FACS (1 µl per test)
Antibody	Anti-CD11b (mouse monoclonal)	eBioscience	Cat#12-0112-82 RRID:AB_2734869	FACS (1 µl per test)
Antibody	Anti-F4/80 (mouse monoclonal)	eBioscience	Cat#17-4801-80 RRID:AB_2784647	FACS (1 µl per test)
Antibody	Anti-Gr-1 (mouse monoclonal)	Biolegend	Cat#108424 RRID:AB_2137485	FACS (1 µl per test)
Antibody	Anti-Ly-6C (mouse monoclonal)	Biolegend	Cat#128022 RRID:AB_10639728	FACS (1 µl per test)
Antibody	Anti-CD11c (mouse monoclonal)	eBioscience	Cat#12-0114-82 RRID:AB_465552	FACS (1 µl per test)
Antibody	Anti-CD45.1 (mouse monoclonal)	eBioscience	Cat#15-0453-82 RRID:AB_468759	FACS (1 µl per test)
Antibody	Anti-CD45.2 (mouse monoclonal)	Biolegend	Cat#109831 RRID:AB_10900256	FACS (1 µl per test)
Antibody	Anti-CD4 (mouse monoclonal)	eBioscience	Cat#12-0041-82 RRID:AB_465506	FACS (1 µl per test)
Antibody	Anti-CD8a (mouse monoclonal)	Biolegend	Cat#100707 RRID:AB_312746	FACS (1 µl per test)
Antibody	Anti-IFN-γ (mouse monoclonal)	Biolegend	Cat#505813 RRID:AB_493312	FACS (1 µl per test)
Antibody	Anti-IL-4 (mouse monoclonal)	Biolegend	Cat#504118 RRID:AB_10898116	FACS (1 µl per test)
Antibody	Anti-CD34 (mouse monoclonal)	eBioscience	Cat#11-0341-82 RRID:AB_465021	FACS (1 µl per test)
Antibody	Anti-Sca-1 (mouse monoclonal)	Biolegend	Cat#108114 RRID:AB_493596	FACS (1 µl per test)
Antibody	Anti-c-Kit (mouse monoclonal)	Biolegend	Cat#105812 RRID:AB_313221	FACS (1 µl per test)
Antibody	Anti-CD135 (mouse monoclonal)	Biolegend	Cat#135314 RRID:AB_2562339	FACS (1 µl per test)
Antibody	Anti-CD3ε (mouse monoclonal)	Biolegend	Cat#100310 RRID:AB_312675	FACS (1 µl per test)
Antibody	Anti-B220 (mouse monoclonal)	Biolegend	Cat#103210 RRID:AB_312995	FACS (1 µl per test)
Antibody	Anti-TER-119 (mouse monoclonal)	Biolegend	Cat#116210 RRID:AB_313711	FACS (1 µl per test)
Antibody	Anti-IgM (mouse monoclonal)	eBioscience	Cat#15-5790-82 RRID:AB_494222	FACS (1 µl per test)
Antibody	Anti-CD16/32 (mouse monoclonal)	Biolegend	Cat#101333 RRID:AB_2563692	FACS (1 µl per test)
Antibody	Anti-CD127 (mouse monoclonal)	Biolegend	Cat#135021 RRID:AB_1937274	FACS (1 µl per test)
Antibody	Anti-TNFα (mouse monoclonal)	Invitrogen	Cat#17-7321-81 RRID:AB_469507	FACS (1 µl per test) IF (1:100)
Antibody	Anti-IL-6 (mouse monoclonal)	Biolegend	Cat#504507 RRID:AB_10694868	FACS (1 µl per test) IF (1:100)
Antibody	Anti-BrdU (mouse monoclonal)	eBioscience	Cat#11-5071-42 RRID:AB_11042627	FACS (1 µl per test)
Antibody	Anti-Endomucin (mouse polyclonal)	R&D	Cat#AF4666	IF (1:100)
Antibody	Anti-CD150 (mouse monoclonal)	Biolegend	Cat#115908 RRID:AB_345278	IF (1:100)
Antibody	Anti-Lineage Panel (mouse monoclonal)	Biolegend	Cat#133307 RRID:AB_11124348	IF (1:100)
Antibody	Anti-Goat AF488 (goat polyclonal)	Invitrogen	Cat#A32814 RRID:AB_2762838	IF (1:1000)
Antibody	Anti-TNF-alpha (mouse monoclonal)	Sino Biological	Cat#50349-R023	2 µg ml^{-1}

Continued on next page

Continued

Reagent type (species) or resource	Designation	Source or reference	Identifiers	Additional information
Antibody	Anti-Rabbit AF488 (rabbit polyclonal)	Invitrogen	Cat#R37118 RRID:AB_2556546	IF (1:1000)
Antibody	Anti-OVA257-264 (SIINFEKL) peptide bound to H-2K^{b} (mouse monoclonal)	Invitrogen	Cat#17-5743-82 RRID:AB_1311286	FACS (1 µl per test)
Antibody	Anti-IL-2 (mouse monoclonal)	eBioscience	Cat#25-7021-80 RRID:AB_1235007	FACS (1 µl per test)
Chemical compound, drug	Diphtheria toxin (DT)	Sigma-Aldrich	Cat#D0564-1MG	40 µg kg^{-1} body mass
Chemical compound, drug	BrdU (5-Bromo-2′-Deoxyuridine)	Sigma-Aldrich	Cat#B5002-250mg	125 mg kg^{-1} body mass
Chemical compound, drug	CFSE (5-Carboxyfluorescein, Succinimidyl Ester)	Invitrogen	Cat#C2210	2.5 µM
Chemical compound, drug	GM-CSF	Abbkine	Cat#PRP2116	10 ng ml^{-1}
Chemical compound, drug	IL-4	novoprotein	Cat#CK15	10 ng ml^{-1}
Chemical compound, drug	Tamoxifen	Sigma-Aldrich	Cat#T5648	20 mg ml^{-1} corn oil
Commercial kit	Chromium Single Cell 3′ GEM, Library & Gel Bead Kit v3	10 x Genomics	PN-1000075	
Commercial kit	Chromium Chip B Single Cell Kit	10 x Genomics	PN-1000074	
Cell line (*Mus musculus*)	NCTC clone 929	ATCC	CCL-1 RRID:CVCL_0462	
Cell line (*Mus musculus*)	B3Z hybridoma CD8 T cell	Dr. Nilabh Shastri		
Other	scRNA sequencing data (raw and processed data)	This paper	GEO: GSE168224	
Genetic reagent (*Mus musculus*)	C57BL/6 J	Shanghai Model Organisms		
Genetic reagent (*Mus musculus*)	Tg(Pf4-icre)Q3Rsko/J (*Pf4^{Cre}*)	Jackson Laboratory	Stock No: 008535	
Genetic reagent (*Mus musculus*)	Gt(ROSA) 26Sortm1(HBEGF) Awai/J (*Rosa26$^{fs\text{-}iDTR}$*)	Jackson Laboratory	Stock No: 007900	
Genetic reagent (*Mus musculus*)	Gt(ROSA)26Sortm4(ACTB-tdTomato,-EGFP)Luo/J (*Rosa26$^{fs\text{-}mTmG}$*)	Jackson Laboratory	Stock No: 007576	
Genetic reagent (*Mus musculus*)	Gt(ROSA)26Sortm9(CAG-tdTomato)Hze/J (*Rosa26$^{fs\text{-}tdTomato}$*)	Jackson Laboratory	Stock No: 007905	
Genetic reagent (*Mus musculus*)	*Scl^{CreER}* mice	***Göthert et al., 2005***		
Genetic reagent (*Mus musculus*)	Cxcl12tm2.1Sjm/J (*Cxcl12$^{fs\text{-}DsRed}$*)	Jackson Laboratory	Stock No: 022458	
Genetic reagent (*Mus musculus*)	C57BL/6-Tg(TcraTcrb)1,100Mjb/J (*OT-I*)	Jackson Laboratory	Stock No: 003831	
Strain, strain background (L. monocytogenes)	10403 S	***Bishop and Hinrichs, 1987***		
Software, algorithm	Cell ranger_3.0.2	10 x Genomics	tenx RRID:SCR_01695	
Software, algorithm	R_3.6.3	https://cran.r-project.org/	R 3.6.3	

Continued on next page

Continued

Reagent type (species) or resource	Designation	Source or reference	Identifiers	Additional information
Software, algorithm	Seurat_3.0.2	**Butler et al., 2018**	Seurat RRID:SCR_016341	
Software, algorithm	ggplot2_3.2.0	https://cran.r-project.org/web/packages/ggplot2/index.html	ggplot2 RRID:SCR_014601	
Software, algorithm	clusterProfiler_3.12.0	**Yu et al., 2012**	clusterProfiler RRID:SCR_016884	
Software, algorithm	pheatmap_1.0.12	https://cran.r-project.org/web/packages/pheatmap/	pheatmap RRID:SCR_016418	
Software, algorithm	CellPhoneDB_2.1.7	**Efremova et al., 2020**	CellPhoneDB RRID:SCR_017054	
Software, algorithm	CellChat_1.1.3	**Jin et al., 2021**	CellChat 1.1.3	
Software, algorithm	symphony_1.0	**Kang et al., 2021**	symphony 1.0	
Software, algorithm	MetaNeighbor_1.10.0	**Crow et al., 2018**	MetaNeighbor RRID:SCR_016727	
Software, algorithm	iMAP_1.0.0	**Wang et al., 2021b**	iMAP 1.0.0	
Software, algorithm	scmap_ 1.16.0	**Kiselev et al., 2018**	Scmap RRID:SCR_017338	
Software, algorithm	enrichplot_1.4.0	**Yu, 2019**	enrichplot 1.4.0	
Software, algorithm	Imaris_8.4	Bitplane	Imaris RRID:SCR_007370	
Software, algorithm	FlowJo_10	BD Bioscience	FlowJo RRID:SCR_008520	
Software, algorithm	ImageJ_ 1.8.0	National Institutes of Health	ImageJ RRID:SCR_003070	
Other	DAPI (4',6-Diamidino-2-Phenylindole, Dihydrochloride)	Thermo Fisher	Cat#D1306	IF (0.5 μg/mL)
Other	Corn oil	Sigma-Aldrich	Cat#PHR2897	Tamoxifen dissolution
Other	Lymphocyte Separation Medium	TBD Science	Cat#LTS1077	Liver cell isolation

Mice

C57BL/6-Tg(*Pf4-cre*)Q3Rsko/J (*Pf4*^{Cre}), C57BL/6-Gt(ROSA) 26Sortm1(HBEGF) Awai/J (*Rosa26*$^{fs\text{-}iDTR}$), C57BL/6-*Gt(ROSA)*26Sortm4(ACTB-tdTomato,-EGFP)Luo/J (*Rosa26*$^{fs\text{-}mTmG}$), Gt(ROSA)26Sortm9(CAG-tdTomato)Hze (*Rosa26*$^{fs\text{-}tdTomato}$), CXCL12tm2.1Sjm/J (*Cxcl12*^{DsRed}) and C57BL/6-Tg(TcraTcrb)1,100Mjb/J (*OT-I*) mice were obtained from the Jackson Laboratory. *Scl*^{CreER} mice were provided by J. R. Göthert. All mice were maintained in the C57BL/6 background. Animals were blindly included in the experiments according to genotyping results as a mix of male and female. All animal experiments were performed according to protocols approved by the Sun Yat-sen University animal care and use committee (approval No. SYSU-IACUC-2021-B0617).

Cell line

B3Z hybridoma T cells were kindly gifted by Dr. Nilabh Shastri (Johns Hopkins University). This cell line was verified to be mycoplasma free by EZdetect PCR Kit for Mycoplasma Detection (HiMedia).

Bacteria and infections

Listeria (*L.*) *monocytogenes* infection was performed as described with minor modifications (**Edelson and Unanue, 2000**; **Verschoor et al., 2011**). In brief, wild-type *L. monocytogenes* strain 10,403 S grown to exponential phase at 37 °C in TSB media was injected intravenously at a dose of 2500 colony-forming units (CFUs) to determine spleen and liver bacterial burdens 3 days after infection. Recombinant *L. monocytogenes* expressing the chicken ovalbumin peptide ($OVA_{257\text{-}264}$) (*L.m.* – $OVA_{257\text{-}264}$) was injected intravenously at a dose of 2500 CFUs to determine activated spleen T cells 7 days after infection. *Escherichia* (*E.*) *coli* wild-type strain 85,344 expressing GFP was constructed as previously described (**Feng et al., 2020**). GFP-labeled *E. coli* was grown to exponential phase at 37 °C in LB media and washed with PBS before being suspended for phagocytosis assays.

Antibodies for flow cytometry analysis and cell sorting

For cell sorting and analysis, monoclonal antibodies to CD41 (MWReg30, eBioscience), CXCR4 (2B11, eBioscience), CD11b (M1/70, eBioscience), F4/80 (BM8, eBioscience), Gr-1 (RB6-8C5, Biolegend),

Ly6C (HK1.4, Biolegend), CD11c (N418, eBioscience), CD45.1 (A20, eBioscience), CD45.2 (104, Biolegend), CD4 (GK1.5, eBioscience), CD8 (53–6.7, Biolegend), INF-γ (XMG1.2, Biolegend), IL4 (11B11, Biolegend), CD34 (RAM34, eBioscience), Sca-1 (D7, Biolegend), c-kit (2B8, Biolegend), CD135 (A2F10, Biolegend), CD3ε (145–2 C11, Biolegend), CD45R (RA3-6B2, Biolegend), TER-119 (Ter-119, Biolegend), IgM (II/41, eBioscience), FγRII (93, Biolegend), IL-7R (A7R34, Biolegend), TNFα (MP6-XT22, Invitrogen), IL-6 (MP5-20F3, Biolegend), OVA257-264 (SIINFEKL) peptide bound to H-2K^{b} (eBio25-D1.16 (25-D1.16), Invitrogen) and IL-2 (JES6-5H4, eBioscience) were used where indicated.

Flow cytometry and cell sorting

Bone marrow cells were isolated from mouse femora and tibiae as previously reported (***Jiang et al., 2018***). Splenocytes were mechanically dissociated in PBS with 2% FBS. Peripheral blood was collected from the retro-orbital sinus and anticoagulated by K2-EDTA. Those three kinds of cells then underwent red blood cell lysis for 5 min using 0.16 M ammonium chloride solution. Liver cells were mechanically dissociated and lysed using 0.16 M ammonium chloride solution, followed by gradient sedimentation using a density reagent (LTS1077, TBD Science) following the manufacturer's instruction. Cell sorting was performed using a cell sorter (MoFlo Astrios, Beckman Coulter) with a 100 μm nozzle at a speed of around 5000 cells s^{-1}. For intracellular cytokine staining, cells were pretreated with Brefeldin-A (BFA, 10 μg ml^{-1}) for 4 hr at 37°C before staining. For MK antigen presentation detection, MKs were co-culture with 100 μg ml^{-1} soluble full-length OVA for 24 hr before staining. For IFNγ, LPS and *L. monocytogenes* treatment, cells were co-culture with 10 ng ml^{-1} IFN-γ or 30 μg ml^{-1} LPS for 4, 18, or 24 hr, or 10^{6} *L. monocytogenes* for 4 hr in a 37°C incubator before staining. Cell analysis was performed on either one of the flow cytometers (Attune NxT, Thermo Fisher; Cytek AURORA, Aurora).

Single-cell library construction and sequencing

Sorted CD41^{+} FSC^{high} single cells from four mice of a control MK group and an MK group from mice 3 days upon *L. monocytogenes* infection each were processed through the Chromium Single Cell Platform using the Chromium Single Cell 3' Library and Gel Bead Kit v3 (PN-1000075, 10 x Genomics) and the Chromium Single Cell B Chip Kit (PN-1000074, 10 x Genomics) as the manufacturer's protocol. In brief, over 7000 cells were loaded onto the Chromium instrument to generate single-cell barcoded droplets. Cells were lysed and barcoded reverse transcription of RNA occurred. The library was prepared by following amplification, fragmentation, adaptor, and index attachment then sequenced on an Illumina NovaSeq platform.

scRNA-seq processing

The scRNA-seq reads were aligned to the mm10 reference genomes, and unique molecular identifier (UMI) counts were obtained by Cell Ranger 3.0.2. Normalization, dimensionality reduction, and clustering were performed with the Seurat 3.0 R package (***Butler et al., 2018***). For the control and *Listeria* (*L.*) *monocytogenes* infection group, we loaded one 10 x Genomics well each and detected 5663 and 5948 cells that passed the Cell Ranger pipeline, respectively. To ruled out low quality cells, cells with >12% mitochondrial content or <200 detected genes were excluded with Seurat function subset (percent.mt <12 & nFeature_RNA >200). We ruled out doublets with default parameters of DoubletDecon R package, and 54 control cells and 939 *L. monocytogenes* infected cells were excluded. Following the standard procedure in Seurat's pipeline, we identified 3272 MKs from control mice (1712 MKs) and mice with *L. monocytogenes* infection (1560 MKs) (3897 and 3449 immune cells were discarded, respectively) in combination with MetaNeighbor method. Preprocessed dataset normalization was performed by dividing the UMI counts per gene by the total UMI counts in the corresponding cell and log-transforming before scaling and centering. SCT normalization was performed with the script: object <- SCTransform(object, vars.to.regress = ""percent.mt"", verbose = FALSE). Signature genes of each cluster were obtained using the Seurat function FindMarkers with Wilcox test with fold change >1.5 and p value <0.05 after clustering. Heatmaps, individual UMAP plots, and violin plots were generated by the Seurat functions in conjunction with ggplot2 and pheatmap R packages.

Similarities and UMAP projection between our scRNA-seq data and published datasets GSE152574 (***Yeung et al., 2020***), GSE158358 (***Pariser et al., 2021***), GSE137540 (***Xie et al., 2020***), GSE128074 (***Hamey et al., 2021***), or GSE132042 (***Almanzar et al., 2020***) were conducted by MetaNeighbor R package (***Crow et al., 2018***), iMAP.py and Symphony R package (***Kang et al., 2021***). iMAP integration

was performed using the default parameters except n_top_genes = 2000, min_genes = 0, min_cells = 0, and n_epochs = 100 before doing dimensionality reduction using Uniform Manifold Approximation and Projection method (UMAP, n_neighbors = 30, n_pca = 30). Radar charts were generated with JavaScript written by Nadieh Bremer (https://www.visualcinnamon.com/). Euclidean distances denote the distances between the centroid of each cluster.

Correlations were calculated based on normalized RNA values, with the function cor and the parameter 'method = "spearman"'. Multiple testing correction using the function cor.test with the parameter "method = "spearman" and it was applied for *Cxcr4* expression correlations. We calculated the similarities between MK1 to 5 with the published MK, immune cell, and myeloid progenitor datasets (**Almanzar et al., 2020**; **Hamey et al., 2021**; **Pariser et al., 2021**; **Xie et al., 2020**; **Yeung et al., 2020**) using scmap R package (**Kiselev et al., 2018**). Default parameters and 1000 features were used and threshold >0 was set. Cell-type matches are selected based on the highest value of similarities and the second-highest value which is not 0.01 less than the highest value across all reference cell types.

Cytokine, inflammatory, chemokine, and antigen processing and presentation scores were evaluated with the AddModuleScore function of Seurat using genes from KEGG pathway ko04060, cytokine-cytokine receptor interaction; GO:0006954, inflammatory response; chemokine ligands from CellPhoneDB.mouse (**Jin et al., 2021**) and GO:0019882, antigen processing and presentation.

Interaction analysis of MKs and immune cells were conducted by CellPhoneDB (**Efremova et al., 2020**) (transformed to human orthologous genes **Davidson et al., 2020**) and CellChat R package (**Jin et al., 2021**). Only interactions involving cytokines were shown. Gene Ontology (GO) analysis was performed using clusterProfiler R package (**Yu et al., 2012**) and visualized using enrichplot R package (**Yu, 2019**).

Gene set enrichment analysis (GSEA) was performed using gsea R package (**Subramanian et al., 2005**) and visualized using enrichplot R package. Gene lists were pre-ranked by the fold change values of the differential expression analysis using Seurat function FindMarkers. Gene sets for GSEA were obtained from GO database (GO:0002367, cytokine production involved in immune response; GO:0006954, inflammatory response; GO:0008009, chemokine activity; GO:0022409, positive regulation of cell-cell adhesion; GO:0002275, myeloid cell activation involved in immune response).

Gene set variation analysis (GSVA) was performed using GSVA R package (**Hänzelmann et al., 2013**). GSVA was performed to calculate GSVA score of indicated pathway genes in single cell datasets with the whole protein encoding genes after log normalization of expression values. Gene sets for GSVA were obtained from GO database (GO:0022409, positive regulation of cell-cell adhesion; GO:0002275, myeloid cell activation involved in immune response; GO:0002367, cytokine production involved in immune response; GO:0007596, blood coagulation; GO:0019882, antigen processing and presentation; GO:0034340: response to type I interferon; GO:0034341: response to interferon-gamma; GO:0045088, regulation of innate immune response; GO:0042742, defense response to bacterium; GO:0002819, regulation of adaptive immune response; GO:1903708, positive regulation of hemopoiesis).

Lung cells preparation for flow cytometry

Lungs were removed and digested as described with minor modifications (**Lefrançais et al., 2017**). In brief, removed lungs were placed in 1.5 ml tubes, minced with scissors, and digested with 1 ml digestion buffer (HBSS with 1 mg ml^{-1} collagenase D, 0.1 mg ml^{-1} DNase I, 25 mM HEPES, 2 mM L-glutamine, and 2% FBS) for 30 min at 37°C before filtration through a 100 μm cell strainer and red blood cell lysis for 5 min. Samples were then filtered through 70 μm strainers and resuspended for subsequent surface marker staining for flow cytometry.

Megakaryocyte ablation induction

Pf4^{Cre} mice were mated with the *Rosa26*$^{fs\text{-}iDTR}$ line to generate *Pf4*^{Cre}*; Rosa26*$^{fs\text{-}iDTR}$ mice. Diphtheria toxin (DT, Sigma-Aldrich) was injected intraperitoneally every day at a dose of 40 ng g^{-1} bodyweight into *Pf4*$^{Cre+}$; *Rosa26*$^{fs\text{-}iDTR+/-}$ mice and their cre negative counterparts to induce megakaryocyte ablation as indicated.

Cre-ER recombinase induction

Scl^{CreER} mice were mated with the *Rosa26*$^{fs\text{-}tdTomato}$ line to generate *Scl*^{CreER}; *Rosa26*$^{fs\text{-}tdTomato}$ mice. For induction of cre-ER recombinase, *Scl*^{CreER}, *Rosa26*$^{fs\text{-}tdTomato+/-}$ mice were injected with tamoxifen intraperitoneally once (2 mg in 0.1 ml corn oil; Sigma-Aldrich).

BrdU incorporation assay

5-Bromo-2-deoxyuridine (BrdU) was administered at a single dose of 125 mg kg^{-1} body mass by intraperitoneal injection. Whole bone marrow cells were collected 12 hr later and incubated with anti-CD41 and anti-CXCR4 for 1 hr. Cells were washed and then fixed with 4% PFA at 4 °C overnight. Cells were then permeabilized with 0.5% TritonX-100 for 15 min at room temperature and incubated with 1 mg ml^{-1} DNase I (Roche) for 1 hr at 37 °C followed by incubating with anti-BrdU (BU20A, eBioscience) for 1 hr at room temperature before being analyzed.

Annexin V binding assay

For Annexin V binding assay, bone marrow cells were incubated with cell surface markers for 1 hr at 4 °C and then washed with PBS before being resuspended with Annexin V binding buffer (Biolegend). Cells were then incubated with FITC Annexin V (Biolegend) for 15 min at room temperature in dark, and then 300 µl Annexin V binding buffer was added to each tube. Cells were analyzed by a flow cytometer.

Immunostaining

Immunostaining of frozen sections was performed as described (***Jiang et al., 2018***). For bone sections, mice were perfused with PBS and 4% paraformaldehyde (PFA). Then the bones were fixed with 4% PFA for 24 hr, decalcified with 0.5 M EDTA for 2 days, and gradient dehydrated by 15% and 30% sucrose for another 2 days. The thick of sections was 30 µm. We used CD41 (MWReg30; eBioscience; 1:200), Endomucin (R&D; 1:100), CD150 (TC15-12F12.2; Biolegend; 1:100), CD48 (HM48-1; Biolegend; 1:100), CXCR4 (2B11, eBioscience; 1:100) antibodies, and lineage panel (Biolegend; cat #133307; 1:50). Secondary staining was done with donkey anti–goat AlexaFluor 488 (Invitrogen; 1:1000). For the liver and spleen from *Pf4*$^{Cre+}$; *Rosa26*$^{fs\text{-}mTmG+/-}$ mice, and lung from *Pf4-cre*$^{+}$; *Rosa26*$^{fs\text{-}tdTomato+/-}$ mice, we used DAPI (Thermo Fisher; 0.5 µg ml^{-1}) to stain the frozen sections. For phagocytosis analysis, F4/80 (BM8, eBioscience; 1:100), CD11b (M1/70; Invitrogen; 1:100), CD41 (MWReg30; Thermo Fisher; 1:200) and DAPI was used. For sorted MKs, we used CXCR4 (2B11, eBioscience; 1:100), TNFα (R023, Sino Biological; 1:100) and IL-6 (MP5-20F3, Biolegend; 1:100) antibody. Secondary staining was performed with donkey anti-rabbit AlexaFluor 488 (Invitrogen; 1:1000). Confocal images were obtained using a spinning-disk confocal microscope (Dragonfly, Andor) and analyzed using Imaris 9.0 software (Oxford Instruments). Three-Dimension plots were generated using Matplotlib (***Hunter, 2007***).

Quantitative real-time (qRT-) PCR

For RT-qPCR, MKs were dissociated in Trizol (Magen), and RNA was extracted following the manufacture's instruction. RNA was reverse transcribed into cDNA using the TransCript All-in-One First-Strand cDNA Synthesis kit (Transgene). Quantitative PCR was performed using a Bio-Rad CFX 96 touch. The primers for *Pf4* were 5′-GGGATCCATCTTAAGCACATCAC-3′ (forward) and 5′-CCATTCTTCAGG GTGGCTATG-3′ (reverse). The primers for *Vwf* were 5′-CTTCTGTACGCCTCAGCTATG-3′ (forward) and 5′-GCCGTTGTAATTCCCACACAAG-3′ (reverse). The primers for *Mpl* were 5′-AACCCGGT ATGTGTGCCAG-3′ (forward) and 5′-AGTTCATGCCTCAGGAAGTCA-3′ (reverse). The primers for *Cxcl12* were 5′-AGGTTCTTATTTCACGGCTTGT-3′ (forward) and 5′-TGGGTGCTGAGACCTTTGAT-3′ (reverse). The primers for *Gapdh* were 5′-AGGTCGGTGTGAACGGATTTG-3′ (forward) and 5′-GGGG TCGTTGATGGCAACA-3′ (reverse). *Gapdh* was used as the reference gene for qRT-PCR analysis.

Transwell migration

Transmigration assays were performed on a transwell with a pore size of 5 µm (Biofil). CXCR4^{low} MKs or CXCR4^{high} MKs from bone marrow were sorted (5000 cells per well) from control mice and added to the lower chamber with 600 µl IMDM (Thermo Fisher) plus 10% FBS (Gibco). Peripheral blood cells were collected as described in the 'Flow cytometry and cell sorting' section. 6×10^{5} peripheral blood

cells were resuspended in 100 µl RPMI 1640 (Gibco) plus 10% FBS and added to the upper insert to continue for 2-hr incubation at 37 °C, 5% CO_2. Cells in the lower chamber were harvested, washed with PBS once, and resuspended with 100 µl PBS for staining and FACS counting.

Phagocytosis

Bone-marrow-derived macrophages (BMDM) from C57BL/6 mice at 6–8 weeks of age were differentiated from bone marrow precursors with minor modifications (***Minutti et al., 2019***). In brief, bone marrow cells were isolated and propagated for 7 days in DMEM without sodium pyruvate or HEPES (Gibco), containing 20% FBS (Gibco), 30% supernatants of L929 conditioned media, and 1% Pen/Strep (Hyclone) at 37 °C. Macrophage phagocytosis assays were performed on a transwell plate with a pore size of 3 µm (Biofil) as described with modifications (***Sharif et al., 2014***). Briefly, attached cells were replated into 24-well plates, 5×10^4 cells per well, on glass coverslips for 24 hr culture. Then 5000 sorted $CXCR4^{low}$ MKs or $CXCR4^{high}$ MKs were added in the upper inserts and placed onto macrophages chambers for additional 16 hr incubation without or with 2 µg ml^{-1} TNFα neutralizing antibody (R023, Sino Biological; 1:100) or 2 µg ml^{-1} IL-6 neutralizing antibody (MP5-20F3, Biolegend) at 37 °C, 5% CO_2. The upper inserts were discarded and macrophages were washed with PBS without antibiotics and incubated with 10^5 GFP-labeled *E. coli* for 2 hr at 37 °C, 5% CO_2. Cells were washed three times with PBS and incubated with DMEM without sodium pyruvate or HEPES (Gibco) with gentamycin (50 µg ml^{-1}) for 30 min at 37 °C, 5% CO_2 to remove adherent bacteria. Cells were then detected by flow cytometry or fixed by cold methanol for 15 min and blocked with 10% BSA overnight, followed by incubation with F4/80 (BM8, eBioscience; 1:100) for 2 hr at room temperature before being quantified using a spinning disk confocal microscope (Dragonfly, Andor).

For neutrophil phagocytosis, $CD11b^+$ $Gr1^+$ $Ly6c^-$ neutrophils were sorted from the spleen and propagated in RPMI 1640 (Gibco) containing 10% FBS. Neutrophil phagocytosis was performed as described in macrophage phagocytosis assay, except cells were sedimented for 30 min and fixed on glass coverslips after incubated with GFP-*E. coli* and gentamycin. The capacity of phagocytosis was evaluated by flow cytometry or by fluorescence intensity of GFP-*E. coli*. using the confocal microscope within macrophages and neutrophils.

For megakaryocyte phagocytosis, $CXCR4^{low}$ and $CXCR4^{high}$ MKs were sorted from the bone marrow and propagated in RPMI 1640 (Gibco) containing 10% FBS without antibiotics and incubated with 10^5 GFP-labeled *E. coli* for 2 hr at 37 °C, 5% CO_2. Cells were washed three times with PBS and incubated with DMEM without sodium pyruvate or HEPES (Gibco) with gentamycin (50 µg ml^{-1}) for 30 min at 37 °C, 5% CO_2 to remove adherent bacteria. Cells were then detected by flow cytometry.

Bone marrow ex vivo live imaging

$Pf4^{Cre+}$; $Rosa26^{fs\text{-}tdTomato+/-}$ mice were infected with *L. monocytogenes* for 24 hr. FITC-Dextran (average mol wt 2000000, Sigma-Aldrich) was injected intravenously at a dose of 1.25 mg per mouse before being sacrificed. The ends of the femur below the end of the marrow cavity were cut. The bone marrow plug was gently flushed out of the end of the bone with a 21-gauge blunt needle not to break up the marrow plug. Bone marrow was flushed integrally and fixed onto a glass slide in a chamber, rinsed with RPMI 1640 (Gibco), and covered slightly with a coverslip. The integrity of the vascular structure in the bone marrow was observed and warranted through FITC-Dextran inflorescence before capturing images. Confocal images were obtained every minute on the spinning-disk confocal microscope (Dragonfly, Andor) and analyzed using Imaris 9.0 software (Oxford Instruments).

In vitro MK culture, MK size, and proplatelet formation measurement

MKs were sorted using a cell sorter (MoFlo Astrios, Beckman Coulter) and cultured in 24-well plates in SFEM (Stem Cell Technologies) plus 100 ng ml^{-1} mTPO (Novoprotein) and 1% Pen/Strep (Hyclone), and incubated at 37 °C, 5% CO_2 for 4 days. Images were taken by a Nikon Ts2R microscope equipped with a Nikon DS-Ri2 camera. Cell size and proplatelet formation were measured on day 3 or day 5 post-cultured, respectively, using Nikon NIS-Elements BR.

Bone marrow transfer experiments

$Pf4^{Cre}$ mice were mated with the $Rosa26^{fs\text{-}tdTomato}$ line to generate $Pf4^{Cre+}$; $Rosa26^{fs\text{-}tdTomato+/-}$ mice. $tdTomato^+$ MKs were isolated from $Pf4^{Cre+}$; $Rosa26^{fs\text{-}tdTomato+/-}$ mice. Six- to 8-week-old recipient mice were

pre-treated with PBS or 2500 CFUs of *L. monocytogenes* as previously described 1 day before cell perfusion. 1×10^5 tdTomato$^+$ MKs were sorted and intravenously injected into control or *L. monocytogenes* infected mice. tdTomato$^+$ MKs were detected in lungs with immunostaining 2 days after cell perfusion.

mtdTomato$^+$ bone marrow cells were isolated from *Pf4*$^{Cre-}$; *Rosa26*$^{fs\text{-}mTmG+/-}$ mice. 1×10^6 mtdTomato$^+$ bone marrow cells were intravenously injected into control or one-day-*L. monocytogenes* infected mice. mtdTomato$^+$ MKs were detected in bone marrow, liver, and spleen 2 days after cell perfusion.

For in vivo CXCR4^{high} MK function assay in MK ablation mice, DT was intraperitoneally injected every day for 5 days. On the second and fourth days, 2×10^5 sorted wild-type CXCR4^{high} MKs or CXCR4^{low} MKs were intravenously injected into indicated groups. PBS or 2500 CFUs of *L. monocytogenes* as previously described were injected intravenously on the third day. Spleen and liver were harvested 3 days after infection to determine the bacterial burdens as described.

T cell reactivation in vitro

Splenocytes (1×10^6 cells well^{-1}) from control or MK ablated mice after 7 days *L.m.*-OVA infection were re-stimulated for 4 hr in vitro with OVA peptide (10 μM) in the presence of Brefeldin-A (BFA, 10 μg ml^{-1}). Activated T cells were then analyzed by a flow cytometer.

For MK-induced T cell activation, 3×10^4 MK subpopulations for each sample were sorted and co-cultured with 100 μg ml^{-1} soluble full-length OVA for 24 hr, then co-cultured with 6×10^4 OT-I CD8$^+$ T cells or B3Z T cells (***Karttunen et al., 1992***) for 48 hr at 37 °C in a 5% CO_2 incubator as described (***Zufferey et al., 2017***). OT-I T cell activation was detected by measuring intracellular IL-2 levels. B3Z T cell activation was detected using β-galactosidase Assay Kit (RG0036, Beyotime). Bone marrow-derived dendritic cells (DCs) were adopted as positive controls for T cell activation assay. To obtain bone marrow-derived DCs, isolated bone marrow cells were cultured in RPMI 1640 with 10 ng ml^{-1} of GM-CSF and 10 ng ml^{-1} of IL-4 as described (***Roney, 2019***).

Computational modeling of random myeloid cell localization

We have performed randomized simulations as in previous reports (***Bruns et al., 2014***; ***Jiang et al., 2018***) in Python. Images of a 400 μm × 400 μm bone marrow region with CXCR4^{high} and CXCR4^{low} MKs, in which background staining was removed, were used to generate MKs onto which 200 myeloid cells were randomly placed, consistent with an average density of 200 myeloid cells per field. Each simulated run placed 200 random myeloid cells (mean diameter 5 μm) was repeated 500 times. The shortest Euclidean distance was calculated for each myeloid cell to CXCR4^{high} or CXCR4^{low} MKs. Random and observed distance distributions were compared using the modified nonparametric two-dimensional (2D) KS test as described (***Bruns et al., 2014***; ***Jiang et al., 2018***).

Statistical analyses

Data are presented as means ± s.e.m or presented medians, first and third quartiles. For phagocytosis assay and MK size measurement, data were analyzed by a one-dimensional KS test. Differences were considered statistically significant if $p<0.05$. For the comparison of three-dimensional distances, a two-dimensional KS test was used. The difference was considered statistically significant if $p<0.05$. For multiple comparisons analysis, data were analyzed by repeated-measures one-way analysis of variance (ANOVA) followed by Dunnett's test. Differences were considered statistically significant if $p<0.05$. ♮ $p<0.05$, ♯ $p<0.01$, ♯♯ $p<0.001$, n.s., not significant. For pairs of measurements, data were analyzed by paired Student's *t*-test. Differences were considered statistically significant if $p<0.05$. # $p<0.05$, ## $p<0.01$, ### $p<0.001$, n.s., not significant. For other experiments except for scRNA-seq analysis, data were analyzed by a two-tailed Student's *t*-test. Differences were considered statistically significant if $p<0.05$. * $p<0.05$, ** $p<0.01$, *** $p<0.001$, n.s., not significant.

Acknowledgements

We thank the National Key Research and Development Program of China (2018YFA0107200), the National Natural Science Foundation of China (82170112, 81900101), The Key Research and Development Program of Guangdong Province (2019B020234002), China Postdoctoral Science Foundation (2021M693614), Guangdong Innovative and Entrepreneurial Research Team Program (2016ZT06S029,

2019ZT08Y485), Sanming Project of Medicine in Shenzhen (No.SZSM201911004) for generous support.

Additional information

Funding

Funder	Grant reference number	Author
National Key Research and Development Program of China	2018YFA0107200	Meng Zhao
National Natural Science Foundation of China	82170112	Meng Zhao
National Natural Science Foundation of China	81900101	Jin Wang
Key Research and Development Program of Guangdong Province	2019B020234002	Meng Zhao
Guangdong Innovative and Entrepreneurial Research Team Program	2016ZT06S029	Meng Zhao
Guangdong Innovative and Entrepreneurial Research Team Program	2019ZT08Y485	Linjia Jiang
Sanming Project of Medicine in Shenzhen	SZSM201911004	Meng Zhao
China Postdoctoral Science Foundation	2021M693614	Jin Wang

The funders had no role in study design, data collection and interpretation, or the decision to submit the work for publication.

Author contributions

Jin Wang, Resources, Data curation, Formal analysis, Funding acquisition, Validation, Investigation, Visualization, Methodology, Writing - original draft, Project administration, Writing - review and editing; Jiayi Xie, Data curation, Formal analysis, Validation, Investigation, Visualization, Methodology, Writing - review and editing; Daosong Wang, Data curation, Investigation, Visualization, Methodology; Xue Han, Minqi Chen, Data curation; Guojun Shi, Linjia Jiang, Supervision; Meng Zhao, Conceptualization, Supervision, Funding acquisition, Writing - original draft, Project administration, Writing - review and editing

Author ORCIDs

Jin Wang http://orcid.org/0000-0002-4924-1716
Jiayi Xie http://orcid.org/0000-0001-8977-6654
Daosong Wang http://orcid.org/0000-0002-4786-6202
Linjia Jiang http://orcid.org/0000-0001-8854-2610
Meng Zhao http://orcid.org/0000-0001-7909-7594

Ethics

All animal experiments were performed according to protocols approved by the Institutional Animal Care and Use Committee.

Decision letter and Author response

Decision letter https://doi.org/10.7554/eLife.78662.sa1
Author response https://doi.org/10.7554/eLife.78662.sa2

Additional files

Supplementary files

- MDAR checklist

Data availability

The scRNA-seq data generated in this study are deposited in GEO (GSE168224, https://www.ncbi.nlm.nih.gov/geo/query/acc.cgi?acc=GSE168224). The code used in the study can be accessed at GitHub (https://github.com/JYCathyXie/MK_infection, copy archived at swh:1:rev:687f151f79a79ad2091e3dc2c5561fc8b4bb347a).

The following dataset was generated:

Author(s)	Year	Dataset title	Dataset URL	Database and Identifier
Zhao M, Wang J, Xie J, Wang D, Han X	2022	Megakaryocyte derived immunoregulatory cells regulate host-defense immunity against bacterial pathogens	https://www.ncbi.nlm.nih.gov/geo/query/acc.cgi?acc=GSE168224	NCBI Gene Expression Omnibus, GSE168224

The following previously published datasets were used:

Author(s)	Year	Dataset title	Dataset URL	Database and Identifier
Yeung AK, Villacorta-Martin C, Murphy GJ	2021	Single Cell Transcriptomic Analysis of Lung and Hematopoietic Megakaryocytes from Embryonic and Adult Mice	https://www.ncbi.nlm.nih.gov/geo/query/acc.cgi?acc=GSE152574	NCBI Gene Expression Omnibus, GSE152574
Pariser DN, Hilt ZT, Ture SK, Blick-Nitko SK, Looney MR, Cleary SJ, Roman-Pagan E, Saunders J, Georas SN, Veazey J, Madera F, Santos LT, Arne A, Huynh NT, Livada AC, Guerrero-Martin SM, Lyons C, Metcalf-Pate KA, McGrath KE, Palis J, Morrell CN	2020	Lung Megakaryocytes are Immune Modulatory Cells	https://www.ncbi.nlm.nih.gov/geo/query/acc.cgi?acc=GSE158358	NCBI Gene Expression Omnibus, GSE158358
Xie X, Shi Q, Wu P, Zhang X	2020	Single-cell transcriptome profiling reveals neutrophil heterogeneity in homeostasis and infection	https://www.ncbi.nlm.nih.gov/geo/query/acc.cgi?acc=GSE137540	NCBI Gene Expression Omnibus, GSE137540
Hamey FK, Lau WW, Diamanti E, Göttgens B, Dahlin JS	2020	Single-cell RNA sequencing of basophils from mouse bone marrow	https://www.ncbi.nlm.nih.gov/geo/query/acc.cgi?acc=GSE128074	NCBI Gene Expression Omnibus, GSE128074
Tabula Muris Consortium	2019	Expression profiling by high throughput sequencing	https://www.ncbi.nlm.nih.gov/geo/query/acc.cgi?acc=GSE132042	NCBI Gene Expression Omnibus, GSE132042

References

Aburima A, Berger M, Spurgeon BEJ, Webb BA, Wraith KS, Febbraio M, Poole AW, Naseem KM. 2021. Thrombospondin-1 promotes hemostasis through modulation of camp signaling in blood platelets. *Blood* **137**:678–689. DOI: https://doi.org/10.1182/blood.2020005382

Almanzar N, Antony J, Baghel AS, Bakerman I. 2020. A single-cell transcriptomic atlas characterizes ageing tissues in the mouse. *Nature* **583**:590–595. DOI: https://doi.org/10.1038/s41586-020-2496-1, PMID: 32669714

Avecilla ST, Hattori K, Heissig B, Tejada R, Liao F, Shido K, Jin DK, Dias S, Zhang F, Hartman TE, Hackett NR, Crystal RG, Witte L, Hicklin DJ, Bohlen P, Eaton D, Lyden D, de Sauvage F, Rafii S. 2004. Chemokine-mediated interaction of hematopoietic progenitors with the bone marrow vascular niche is required for thrombopoiesis. *Nature Medicine* **10**:64–71. DOI: https://doi.org/10.1038/nm973, PMID: 14702636

Beaulieu LM, Lin E, Morin KM, Tanriverdi K, Freedman JE. 2011. Regulatory effects of TLR2 on megakaryocytic cell function. *Blood* **117**:5963–5974. DOI: https://doi.org/10.1182/blood-2010-09-304949, PMID: 21454454

Bernardes JP, Mishra N, Tran F, Bahmer T, Best L, Blase JI, Bordoni D, Franzenburg J, Geisen U, Josephs-Spaulding J, Köhler P, Künstner A, Rosati E, Aschenbrenner AC, Bacher P, Baran N, Boysen T, Brandt B, Bruse N, Dörr J, et al. 2020. Longitudinal multi-omics analyses identify responses of megakaryocytes, erythroid cells, and plasmablasts as hallmarks of severe COVID-19. *Immunity* **53**:1296–1314.. DOI: https://doi.org/10.1016/j.immuni.2020.11.017, PMID: 33296687

Bishop DK, Hinrichs DJ. 1987. Adoptive transfer of immunity to Listeria monocytogenes The influence of in vitro stimulation on lymphocyte subset requirements. *Journal of Immunology* **139**:2005–2009 PMID: 3114382.

Boilard E, Machlus KR. 2021. Location is everything when it comes to megakaryocyte function. *The Journal of Clinical Investigation* **131**:144964. DOI: https://doi.org/10.1172/JCI144964, PMID: 33393510

Bruns I, Lucas D, Pinho S, Ahmed J, Lambert MP, Kunisaki Y, Scheiermann C, Schiff L, Poncz M, Bergman A, Frenette PS. 2014. Megakaryocytes regulate hematopoietic stem cell quiescence through CXCL4 secretion. *Nature Medicine* **20**:1315–1320. DOI: https://doi.org/10.1038/nm.3707, PMID: 25326802

Butler A, Hoffman P, Smibert P, Papalexi E, Satija R. 2018. Integrating single-cell transcriptomic data across different conditions, technologies, and species. *Nature Biotechnology* **36**:411–420. DOI: https://doi.org/10.1038/nbt.4096, PMID: 29608179

Campbell RA, Schwertz H, Hottz ED, Rowley JW, Manne BK, Washington AV, Hunter-Mellado R, Tolley ND, Christensen M, Eustes AS, Montenont E, Bhatlekar S, Ventrone CH, Kirkpatrick BD, Pierce KK, Whitehead SS, Diehl SA, Bray PF, Zimmerman GA, Kosaka Y, et al. 2019. Human megakaryocytes possess intrinsic antiviral immunity through regulated induction of IFITM3. *Blood* **133**:2013–2026. DOI: https://doi.org/10.1182/blood-2018-09-873984, PMID: 30723081

Chang Y, Bluteau D, Debili N, Vainchenker W. 2007. From hematopoietic stem cells to platelets. *Journal of Thrombosis and Haemostasis* **5 Suppl 1**:318–327. DOI: https://doi.org/10.1111/j.1538-7836.2007.02472.x, PMID: 17635743

Couldwell G, Machlus KR. 2019. Modulation of megakaryopoiesis and platelet production during inflammation. *Thrombosis Research* **179**:114–120. DOI: https://doi.org/10.1016/j.thromres.2019.05.008, PMID: 31128560

Crow M, Paul A, Ballouz S, Huang ZJ, Gillis J. 2018. Characterizing the replicability of cell types defined by single cell RNA-sequencing data using MetaNeighbor. *Nature Communications* **9**:884. DOI: https://doi.org/10.1038/s41467-018-03282-0, PMID: 29491377

Cunin P, Penke LR, Thon JN, Monach PA, Jones T, Chang MH, Chen MM, Melki I, Lacroix S, Iwakura Y, Ware J, Gurish MF, Italiano JE, Boilard E, Nigrovic PA. 2017. Megakaryocytes compensate for Kit insufficiency in murine arthritis. *The Journal of Clinical Investigation* **127**:1714–1724. DOI: https://doi.org/10.1172/JCI84598, PMID: 28375155

Cunin P, Nigrovic PA. 2019. Megakaryocytes as immune cells. *Journal of Leukocyte Biology* **105**:1111–1121. DOI: https://doi.org/10.1002/JLB.MR0718-261RR, PMID: 30645026

Davidson S, Efremova M, Riedel A, Mahata B, Pramanik J, Huuhtanen J, Kar G, Vento-Tormo R, Hagai T, Chen X, Haniffa MA, Shields JD, Teichmann SA. 2020. Single-cell rna sequencing reveals a dynamic stromal niche that supports tumor growth. *Cell Reports* **31**:107628. DOI: https://doi.org/10.1016/j.celrep.2020.107628, PMID: 32433953

Davis RE, Stenberg PE, Levin J, Beckstead JH. 1997. Localization of megakaryocytes in normal mice and following administration of platelet antiserum, 5-fluorouracil, or radiostrontium: evidence for the site of platelet production. *Experimental Hematology* **25**:638–648 PMID: 9216740.

Deutsch VR, Tomer A. 2006. Megakaryocyte development and platelet production. *British Journal of Haematology* **134**:453–466. DOI: https://doi.org/10.1111/j.1365-2141.2006.06215.x, PMID: 16856888

Deutsch VR, Tomer A. 2013. Advances in megakaryocytopoiesis and thrombopoiesis: from bench to bedside. *British Journal of Haematology* **161**:778–793. DOI: https://doi.org/10.1111/bjh.12328, PMID: 23594368

Dominici M, Rasini V, Bussolari R, Chen X, Hofmann TJ, Spano C, Bernabei D, Veronesi E, Bertoni F, Paolucci P, Conte P, Horwitz EM. 2009. Restoration and reversible expansion of the osteoblastic hematopoietic stem cell niche after marrow radioablation. *Blood* **114**:2333–2343. DOI: https://doi.org/10.1182/blood-2008-10-183459, PMID: 19433859

Dong F, Hao S, Zhang S, Zhu C, Cheng H, Yang Z, Hamey FK, Wang X, Gao A, Wang F, Gao Y, Dong J, Wang C, Wang J, Lan Y, Liu B, Ema H, Tang F, Göttgens B, Zhu P, et al. 2020. Differentiation of transplanted haematopoietic stem cells tracked by single-cell transcriptomic analysis. *Nature Cell Biology* **22**:630–639. DOI: https://doi.org/10.1038/s41556-020-0512-1, PMID: 32367048

Eash KJ, Means JM, White DW, Link DC. 2009. CXCR4 is a key regulator of neutrophil release from the bone marrow under basal and stress granulopoiesis conditions. *Blood* **113**:4711–4719. DOI: https://doi.org/10.1182/blood-2008-09-177287, PMID: 19264920

Edelson BT, Unanue ER. 2000. Immunity to Listeria infection. *Current Opinion in Immunology* **12**:425–431. DOI: https://doi.org/10.1016/s0952-7915(00)00112-6, PMID: 10899025

Efremova M, Vento-Tormo M, Teichmann SA, Vento-Tormo R. 2020. CellPhoneDB: inferring cell-cell communication from combined expression of multi-subunit ligand-receptor complexes. *Nature Protocols* **15**:1484–1506. DOI: https://doi.org/10.1038/s41596-020-0292-x, PMID: 32103204

Feng S, Liu Y, Liang W, El-Sayed Ahmed M, Zhao Z, Shen C, Roberts AP, Liang L, Liao L, Zhong Z, Guo Z, Yang Y, Wen X, Chen H, Tian GB. 2020. Involvement of transcription elongation factor grea in mycobacterium viability, antibiotic susceptibility, and intracellular fitness. *Frontiers in Microbiology* **11**:413. DOI: https://doi.org/10.3389/fmicb.2020.00413, PMID: 32265867

Finkielsztein A, Schlinker AC, Zhang L, Miller WM, Datta SK. 2015. Human megakaryocyte progenitors derived from hematopoietic stem cells of normal individuals are MHC class II-expressing professional APC that enhance Th17 and Th1/Th17 responses. *Immunology Letters* **163**:84–95. DOI: https://doi.org/10.1016/j.imlet.2014.11.013, PMID: 25454068

Fuentes R, Wang YH, Hirsch J, Wang C, Rauova L, Worthen GS, Kowalska MA, Poncz M. 2010. Infusion of mature megakaryocytes into mice yields functional platelets. *The Journal of Clinical Investigation* **120**:3917–3922. DOI: https://doi.org/10.1172/JCI43326, PMID: 20972336

Göthert JR, Gustin SE, Hall MA, Green AR, Göttgens B, Izon DJ, Begley CG. 2005. In vivo fate-tracing studies using the Scl stem cell enhancer: embryonic hematopoietic stem cells significantly contribute to adult hematopoiesis. *Blood* **105**:2724–2732. DOI: https://doi.org/10.1182/blood-2004-08-3037, PMID: 15598809

Haas S, Hansson J, Klimmeck D, Loeffler D, Velten L, Uckelmann H, Wurzer S, Prendergast ÁM, Schnell A, Hexel K, Santarella-Mellwig R, Blaszkiewicz S, Kuck A, Geiger H, Milsom MD, Steinmetz LM, Schroeder T, Trumpp A, Krijgsveld J, Essers MAG. 2015. Inflammation-induced emergency megakaryopoiesis driven by hematopoietic stem cell-like megakaryocyte progenitors. *Cell Stem Cell* **17**:422–434. DOI: https://doi.org/10.1016/j.stem.2015.07.007, PMID: 26299573

Hamada T, Möhle R, Hesselgesser J, Hoxie J, Nachman RL, Moore MA, Rafii S. 1998. Transendothelial migration of megakaryocytes in response to stromal cell-derived factor 1 (SDF-1) enhances platelet formation. *The Journal of Experimental Medicine* **188**:539–548. DOI: https://doi.org/10.1084/jem.188.3.539, PMID: 9687531

Hamey FK, Lau WWY, Kucinski I, Wang X, Diamanti E, Wilson NK, Göttgens B, Dahlin JS. 2021. Single-cell molecular profiling provides a high-resolution map of basophil and mast cell development. *Allergy* **76**:1731–1742. DOI: https://doi.org/10.1111/all.14633, PMID: 33078414

Hänzelmann S, Castelo R, Guinney J. 2013. GSVA: gene set variation analysis for microarray and RNA-Seq data. *BMC Bioinformatics* **14**:7. DOI: https://doi.org/10.1186/1471-2105-14-7, PMID: 23323831

Hérault A, Binnewies M, Leong S, Calero-Nieto FJ, Zhang SY, Kang YA, Wang X, Pietras EM, Chu SH, Barry-Holson K, Armstrong S, Göttgens B, Passegué E. 2017. Myeloid progenitor cluster formation drives emergency and leukaemic myelopoiesis. *Nature* **544**:53–58. DOI: https://doi.org/10.1038/nature21693, PMID: 28355185

Hunter JD. 2007. Matplotlib: a 2d graphics environment. *Computing in Science & Engineering* **9**:90–95. DOI: https://doi.org/10.1109/MCSE.2007.55

Itkin T, Gur-Cohen S, Spencer JA, Schajnovitz A, Ramasamy SK, Kusumbe AP, Ledergor G, Jung Y, Milo I, Poulos MG, Kalinkovich A, Ludin A, Golan K, Khatib E, Kumari A, Kollet O, Shakhar G, Butler JM, Rafii S, Adams RH, et al. 2016. Distinct bone marrow blood vessels differentially regulate haematopoiesis. *Nature* **532**:323–328. DOI: https://doi.org/10.1038/nature17624, PMID: 27074509

Jiang L, Han X, Wang J, Wang C, Sun X, Xie J, Wu G, Phan H, Liu Z, Yeh ETH, Zhang C, Zhao M, Kang X. 2018. SHP-1 regulates hematopoietic stem cell quiescence by coordinating TGF-β signaling. *Journal of Experimental Medicine* **215**:1337–1347. DOI: https://doi.org/10.1084/jem.20171477, PMID: 29669741

Jin S, Guerrero-Juarez CF, Zhang L, Chang I, Ramos R, Kuan CH, Myung P, Plikus MV, Nie Q. 2021. Inference and analysis of cell-cell communication using CellChat. *Nature Communications* **12**:1088. DOI: https://doi.org/10.1038/s41467-021-21246-9, PMID: 33597522

Kanaji S, Kanaji T, Jacquelin B, Chang M, Nugent DJ, Komatsu N, Moroi M, Izuhara K, Kunicki TJ. 2005. Thrombopoietin initiates demethylation-based transcription of GP6 during megakaryocyte differentiation. *Blood* **105**:3888–3892. DOI: https://doi.org/10.1182/blood-2004-08-3109, PMID: 15701720

Kang JB, Nathan A, Weinand K, Zhang F, Millard N, Rumker L, Moody DB, Korsunsky I, Raychaudhuri S. 2021. Efficient and precise single-cell reference atlas mapping with Symphony. *Nature Communications* **12**:5890. DOI: https://doi.org/10.1038/s41467-021-25957-x, PMID: 34620862

Karttunen J, Sanderson S, Shastri N. 1992. Detection of rare antigen-presenting cells by the lacZ T-cell activation assay suggests an expression cloning strategy for T-cell antigens. *PNAS* **89**:6020–6024. DOI: https://doi.org/10.1073/pnas.89.13.6020, PMID: 1378619

Kiselev VY, Yiu A, Hemberg M. 2018. scmap: projection of single-cell RNA-seq data across data sets. *Nature Methods* **15**:359–362. DOI: https://doi.org/10.1038/nmeth.4644, PMID: 29608555

Köhler A, De Filippo K, Hasenberg M, van den Brandt C, Nye E, Hosking MP, Lane TE, Männ L, Ransohoff RM, Hauser AE, Winter O, Schraven B, Geiger H, Hogg N, Gunzer M. 2011. G-CSF-mediated thrombopoietin release triggers neutrophil motility and mobilization from bone marrow via induction of Cxcr2 ligands. *Blood* **117**:4349–4357. DOI: https://doi.org/10.1182/blood-2010-09-308387, PMID: 21224471

Lefrançais E, Ortiz-Muñoz G, Caudrillier A, Mallavia B, Liu F, Sayah DM, Thornton EE, Headley MB, David T, Coughlin SR, Krummel MF, Leavitt AD, Passegué E, Looney MR. 2017. The lung is a site of platelet biogenesis and a reservoir for haematopoietic progenitors. *Nature* **544**:105–109. DOI: https://doi.org/10.1038/nature21706, PMID: 28329764

Li B, Jones LL, Geiger TL. 2018. IL-6 promotes t cell proliferation and expansion under inflammatory conditions in association with low-level roryt expression. *Journal of Immunology* **201**:2934–2946. DOI: https://doi.org/10.4049/jimmunol.1800016, PMID: 30315140

Liu C, Wu D, Xia M, Li M, Sun Z, Shen B, Liu Y, Jiang E, Wang H, Su P, Shi L, Xiao Z, Zhu X, Zhou W, Wang Q, Gao X, Cheng T, Zhou J. 2021. Characterization of cellular heterogeneity and an immune subpopulation of

human megakaryocytes. *Advanced Science* **8**:e2100921. DOI: https://doi.org/10.1002/advs.202100921, PMID: 34042332

Machlus KR, Italiano JE. 2013. The incredible journey: From megakaryocyte development to platelet formation. *The Journal of Cell Biology* **201**:785–796. DOI: https://doi.org/10.1083/jcb.201304054, PMID: 23751492

Markovic B, Wu Z, Chesterman CN, Chong BH. 1995. Quantitation of soluble and membrane-bound Fc gamma RIIA (CD32A) mRNA in platelets and megakaryoblastic cell line (Meg-01). *British Journal of Haematology* **91**:37–42. DOI: https://doi.org/10.1111/j.1365-2141.1995.tb05241.x, PMID: 7577649

Minutti CM, Modak RV, Macdonald F, Li FQ, Smyth DJ, Dorward DA, Blair N, Husovsky C, Muir A, Giampazolias E, Dobie R, Maizels RM, Kendall TJ, Griggs DW, Kopf M, Henderson NC, Zaiss DM. 2019. A macrophage-pericyte axis directs tissue restoration via amphiregulin-induced transforming growth factor beta activation. *Immunity* **50**:645–654.. DOI: https://doi.org/10.1016/j.immuni.2019.01.008, PMID: 30770250

Nagata Y, Muro Y, Todokoro K. 1997. Thrombopoietin-induced polyploidization of bone marrow megakaryocytes is due to a unique regulatory mechanism in late mitosis. *The Journal of Cell Biology* **139**:449–457. DOI: https://doi.org/10.1083/jcb.139.2.449, PMID: 9334347

Navarro S, Debili N, Le Couedic JP, Klein B, Breton-Gorius J, Doly J, Vainchenker W. 1991. Interleukin-6 and its receptor are expressed by human megakaryocytes: in vitro effects on proliferation and endoreplication. *Blood* **77**:461–471 PMID: 1991163.

Negrotto S, J De Giusti C, Lapponi MJ, Etulain J, Rivadeneyra L, Pozner RG, Gomez RM, Schattner M. 2011. Expression and functionality of type I interferon receptor in the megakaryocytic lineage. *Journal of Thrombosis and Haemostasis* **9**:2477–2485. DOI: https://doi.org/10.1111/j.1538-7836.2011.04530.x, PMID: 22136495

Nishimura S, Nagasaki M, Kunishima S, Sawaguchi A, Sakata A, Sakaguchi H, Ohmori T, Manabe I, Italiano JE, Ryu T, Takayama N, Komuro I, Kadowaki T, Eto K, Nagai R. 2015. IL-1α induces thrombopoiesis through megakaryocyte rupture in response to acute platelet needs. *The Journal of Cell Biology* **209**:453–466. DOI: https://doi.org/10.1083/jcb.201410052, PMID: 25963822

Olson TS, Caselli A, Otsuru S, Hofmann TJ, Williams R, Paolucci P, Dominici M, Horwitz EM. 2013. Megakaryocytes promote murine osteoblastic HSC niche expansion and stem cell engraftment after radioablative conditioning. *Blood* **121**:5238–5249. DOI: https://doi.org/10.1182/blood-2012-10-463414, PMID: 23667055

Ozaki Y, Asazuma N, Suzuki-Inoue K, Berndt MC. 2005. Platelet gpib-IX-V-dependent signaling. *Journal of Thrombosis and Haemostasis* **3**:1745–1751. DOI: https://doi.org/10.1111/j.1538-7836.2005.01379.x, PMID: 16102041

Pal K, Nowak R, Billington N, Liu R, Ghosh A, Sellers JR, Fowler VM. 2020. Megakaryocyte migration defects due to nonmuscle myosin IIA mutations underlie thrombocytopenia in MYH9-related disease. *Blood* **135**:1887–1898. DOI: https://doi.org/10.1182/blood.2019003064, PMID: 32315395

Pariser DN, Hilt ZT, Ture SK, Blick-Nitko SK, Looney MR, Cleary SJ, Roman-Pagan E, Saunders J, Georas SN, Veazey J, Madere F, Santos LT, Arne A, Huynh NP, Livada AC, Guerrero-Martin SM, Lyons C, Metcalf-Pate KA, McGrath KE, Palis J, et al. 2021. Lung megakaryocytes are immune modulatory cells. *The Journal of Clinical Investigation* **131**:137377. DOI: https://doi.org/10.1172/JCI137377, PMID: 33079726

Patel SR, Hartwig JH, Italiano JE. 2005. The biogenesis of platelets from megakaryocyte proplatelets. *The Journal of Clinical Investigation* **115**:3348–3354. DOI: https://doi.org/10.1172/JCI26891, PMID: 16322779

Ren X, Wen W, Fan X, Hou W, Su B, Cai P, Li J, Liu Y, Tang F, Zhang F, Yang Y, He J, Ma W, He J, Wang P, Cao Q, Chen F, Chen Y, Cheng X, Deng G, et al. 2021. COVID-19 immune features revealed by a large-scale single-cell transcriptome atlas. *Cell* **184**:1895–1913.. DOI: https://doi.org/10.1016/j.cell.2021.01.053, PMID: 33657410

Roney K. 2019. Bone marrow-derived dendritic cells. Allen IC (Ed). *Mouse Models of Innate Immunity: Methods and Protocols*. New York: Springer. p. 57–62.

Rothe, G., Kellermann, W., Briegel, J., Schaerer, B., & Valet, G. (1993). Activation of Neutrophils by Tumor Necrosis Factor-α During Sepsis. In E. Faist, J. L. Meakins, & F. W. Schildberg (Eds.), Host Defense Dysfunction in Trauma, Shock and Sepsis: Mechanisms and Therapeutic Approaches (pp. 727-735). Springer Berlin Heidelberg.

Saçma M, Pospiech J, Bogeska R, de Back W, Mallm J-P, Sakk V, Soller K, Marka G, Vollmer A, Karns R, Cabezas-Wallscheid N, Trumpp A, Méndez-Ferrer S, Milsom MD, Mulaw MA, Geiger H, Florian MC. 2019. Haematopoietic stem cells in perisinusoidal niches are protected from ageing. *Nature Cell Biology* **21**:1309–1320. DOI: https://doi.org/10.1038/s41556-019-0418-y, PMID: 31685996

Semple JW, Italiano JE, Freedman J. 2011. Platelets and the immune continuum. *Nature Reviews. Immunology* **11**:264–274. DOI: https://doi.org/10.1038/nri2956, PMID: 21436837

Shapouri-Moghaddam A, Mohammadian S, Vazini H, Taghadosi M, Esmaeili SA, Mardani F, Seifi B, Mohammadi A, Afshari JT, Sahebkar A. 2018. Macrophage plasticity, polarization, and function in health and disease. *Journal of Cellular Physiology* **233**:6425–6440. DOI: https://doi.org/10.1002/jcp.26429, PMID: 29319160

Sharif O, Gawish R, Warszawska JM, Martins R, Lakovits K, Hladik A, Doninger B, Brunner J, Korosec A, Schwarzenbacher RE, Berg T, Kralovics R, Colinge J, Mesteri I, Gilfillan S, Salmaggi A, Verschoor A, Colonna M, Knapp S. 2014. The triggering receptor expressed on myeloid cells 2 inhibits complement component 1q effector mechanisms and exerts detrimental effects during pneumococcal pneumonia. *PLOS Pathogens* **10**:e1004167. DOI: https://doi.org/10.1371/journal.ppat.1004167, PMID: 24945405

Stephenson E, Reynolds G, Botting RA, Calero-Nieto FJ, Morgan MD, Tuong ZK, Bach K, Sungnak W, Worlock KB, Yoshida M, Kumasaka N, Kania K, Engelbert J, Olabi B, Spegarova JS, Wilson NK, Mende N,

Jardine L, Gardner LCS, Goh I, et al. 2021. Single-cell multi-omics analysis of the immune response in COVID-19. *Nature Medicine* **27**:904–916. DOI: https://doi.org/10.1038/s41591-021-01329-2, PMID: 33879890

Subramanian A, Tamayo P, Mootha VK, Mukherjee S, Ebert BL, Gillette MA, Paulovich A, Pomeroy SL, Golub TR, Lander ES, Mesirov JP. 2005. Gene set enrichment analysis: a knowledge-based approach for interpreting genome-wide expression profiles. *PNAS* **102**:15545–15550. DOI: https://doi.org/10.1073/pnas.0506580102, PMID: 16199517

Sugiyama T, Kohara H, Noda M, Nagasawa T. 2006. Maintenance of the hematopoietic stem cell pool by CXCL12-CXCR4 chemokine signaling in bone marrow stromal cell niches. *Immunity* **25**:977–988. DOI: https://doi.org/10.1016/j.immuni.2006.10.016, PMID: 17174120

Sun S, Jin C, Si J, Lei Y, Chen K, Cui Y, Liu Z, Liu J, Zhao M, Zhang X, Tang F, Rondina MT, Li Y, Wang QF. 2021. Single-cell analysis of ploidy and the transcriptome reveals functional and spatial divergency in murine megakaryopoiesis. *Blood* **138**:1211–1224. DOI: https://doi.org/10.1182/blood.2021010697, PMID: 34115843

Suraneni PK, Corey SJ, Hession MJ, Ishaq R, Awomolo A, Hasan S, Shah C, Liu H, Wickrema A, Debili N, Crispino JD, Eklund EA, Chen Y. 2018. Dynamins 2 and 3 control the migration of human megakaryocytes by regulating CXCR4 surface expression and ITGB1 activity. *Blood Advances* **2**:3540–3552. DOI: https://doi.org/10.1182/bloodadvances.2018021923, PMID: 30538113

Tamura S, Suzuki-Inoue K, Tsukiji N, Shirai T, Sasaki T, Osada M, Satoh K, Ozaki Y. 2016. Podoplanin-positive periarteriolar stromal cells promote megakaryocyte growth and proplatelet formation in mice by CLEC-2. *Blood* **127**:1701–1710. DOI: https://doi.org/10.1182/blood-2015-08-663708, PMID: 26796360

Tiedt R, Schomber T, Hao-Shen H, Skoda RC. 2007. Pf4-Cre transgenic mice allow the generation of lineage-restricted gene knockouts for studying megakaryocyte and platelet function in vivo. *Blood* **109**:1503–1506. DOI: https://doi.org/10.1182/blood-2006-04-020362, PMID: 17032923

Verschoor A, Neuenhahn M, Navarini AA, Graef P, Plaumann A, Seidlmeier A, Nieswandt B, Massberg S, Zinkernagel RM, Hengartner H, Busch DH. 2011. A platelet-mediated system for shuttling blood-borne bacteria to CD8α+ dendritic cells depends on glycoprotein GPIb and complement C3. *Nature Immunology* **12**:1194–1201. DOI: https://doi.org/10.1038/ni.2140, PMID: 22037602

Wang JF, Liu ZY, Groopman JE. 1998. The alpha-chemokine receptor CXCR4 is expressed on the megakaryocytic lineage from progenitor to platelets and modulates migration and adhesion. *Blood* **92**:756–764 PMID: 9680341.

Wang H, He J, Xu C, Chen X, Yang H, Shi S, Liu C, Zeng Y, Wu D, Bai Z, Wang M, Wen Y, Su P, Xia M, Huang B, Ma C, Bian L, Lan Y, Cheng T, Shi L, et al. 2021a. Decoding human megakaryocyte development. *Cell Stem Cell* **28**:535–549. DOI: https://doi.org/10.1016/j.stem.2020.11.006, PMID: 33340451

Wang D, Hou S, Zhang L, Wang X, Liu B, Zhang Z. 2021b. IMAP: integration of multiple single-cell datasets by adversarial paired transfer networks. *Genome Biology* **22**:63. DOI: https://doi.org/10.1186/s13059-021-02280-8, PMID: 33602306

Ward JR, Bingle L, Judge HM, Brown SB, Storey RF, Whyte MKB, Dower SK, Buttle DJ, Sabroe I. 2005. Agonists of toll-like receptor (TLR)2 and TLR4 are unable to modulate platelet activation by adenosine diphosphate and platelet activating factor. *Thrombosis and Haemostasis* **94**:831–838 PMID: 16270639.

Xie Y, Yin T, Wiegraebe W, He XC, Miller D, Stark D, Perko K, Alexander R, Schwartz J, Grindley JC, Park J, Haug JS, Wunderlich JP, Li H, Zhang S, Johnson T, Feldman RA, Li L. 2009. Detection of functional haematopoietic stem cell niche using real-time imaging. *Nature* **457**:97–101. DOI: https://doi.org/10.1038/nature07639, PMID: 19052548

Xie X, Shi Q, Wu P, Zhang X, Kambara H, Su J, Yu H, Park SY, Guo R, Ren Q, Zhang S, Xu Y, Silberstein LE, Cheng T, Ma F, Li C, Luo HR. 2020. Single-cell transcriptome profiling reveals neutrophil heterogeneity in homeostasis and infection. *Nature Immunology* **21**:1119–1133. DOI: https://doi.org/10.1038/s41590-020-0736-z, PMID: 32719519

Yamazaki S, Ema H, Karlsson G, Yamaguchi T, Miyoshi H, Shioda S, Taketo MM, Karlsson S, Iwama A, Nakauchi H. 2011. Nonmyelinating Schwann cells maintain hematopoietic stem cell hibernation in the bone marrow niche. *Cell* **147**:1146–1158. DOI: https://doi.org/10.1016/j.cell.2011.09.053, PMID: 22118468

Yang M, Li K, Chui CM, Yuen PM, Chan PK, Chuen CK, Li CK, Fok TF. 2000. Expression of interleukin (IL) 1 type I and type II receptors in megakaryocytic cells and enhancing effects of IL-1beta on megakaryocytopoiesis and NF-E2 expression. *British Journal of Haematology* **111**:371–380. DOI: https://doi.org/10.1046/j.1365-2141.2000.02340.x, PMID: 11091227

Yeung AK, Villacorta-Martin C, Hon S, Rock JR, Murphy GJ. 2020. Lung megakaryocytes display distinct transcriptional and phenotypic properties. *Blood Advances* **4**:6204–6217. DOI: https://doi.org/10.1182/bloodadvances.2020002843, PMID: 33351116

Yu G, Wang LG, Han Y, He QY. 2012. clusterProfiler: an R package for comparing biological themes among gene clusters. *Omics: A Journal of Integrative Biology* **16**:284–287. DOI: https://doi.org/10.1089/omi.2011.0118, PMID: 22455463

Yu G. 2019. enrichplot: Visualization of Functional Enrichment Result. Enrichplot. https://github.com/GuangchuangYu/enrichplot

Zhao M, Perry JM, Marshall H, Venkatraman A, Qian P, He XC, Ahamed J, Li L. 2014. Megakaryocytes maintain homeostatic quiescence and promote post-injury regeneration of hematopoietic stem cells. *Nature Medicine* **20**:1321–1326. DOI: https://doi.org/10.1038/nm.3706, PMID: 25326798

Zufferey A, Speck ER, Machlus KR, Aslam R, Guo L, McVey MJ, Kim M, Kapur R, Boilard E, Italiano JE, Semple JW. 2017. Mature murine megakaryocytes present antigen-MHC class I molecules to T cells and

transfer them to platelets. *Blood Advances* **1**:1773–1785. DOI: https://doi.org/10.1182/bloodadvances.2017007021, PMID: 29296823